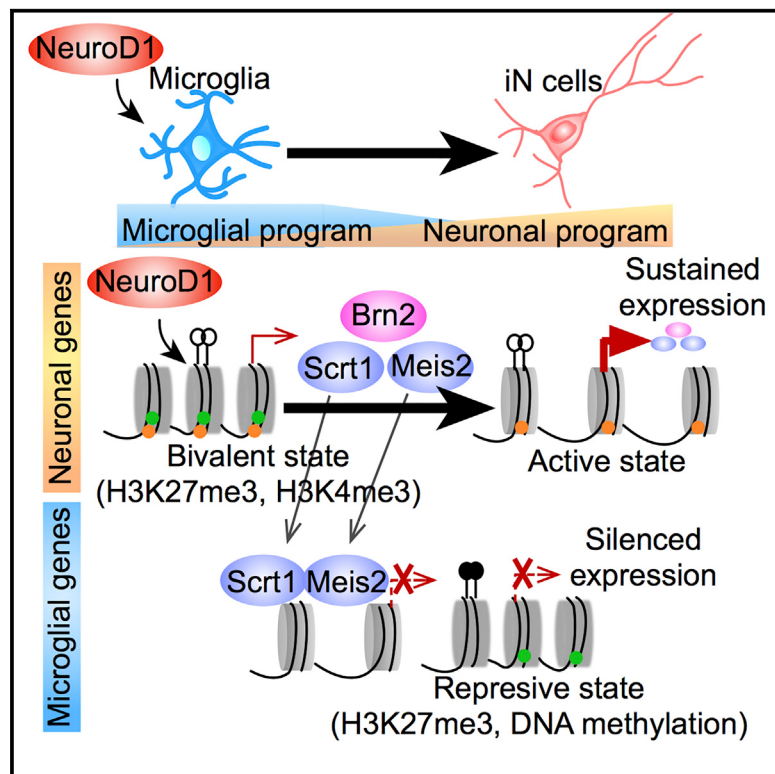


Neuron

Pioneer Factor NeuroD1 Rearranges Transcriptional and Epigenetic Profiles to Execute Microglia-Neuron Conversion

Graphical Abstract



Authors

Taito Matsuda, Takashi Irie,
Shutaro Katsurabayashi, ...,
Katsunori Iwasaki, Takuya Imamura,
Kinichi Nakashima

Correspondence

[\(T.M.\),](mailto:tmatsuda@scb.med.kyushu-u.ac.jp)
[\(K.N.\)](mailto:kin1@scb.med.kyushu-u.ac.jp)

In Brief

Matsuda et al. report direct neuronal conversion of microglia induced by the expression of a single transcription factor, NeuroD1, which occupies bivalent epigenetic domains for neuronal gene induction. NeuroD1 can also convert microglia into neurons in the adult mouse striatum.

Highlights

- NeuroD1 occupies bivalent domains for neuronal gene induction
- NeuroD1 alters the epigenome to control neuronal conversion from microglia
- NeuroD1 initiates the neuronal program prior to suppressing the microglial program
- NeuroD1 converts microglia into neurons in the adult mouse striatum



Pioneer Factor NeuroD1 Rearranges Transcriptional and Epigenetic Profiles to Execute Microglia–Neuron Conversion

Taito Matsuda,^{1,*} Takashi Irie,¹ Shutaro Katsurabayashi,^{2,8} Yoshinori Hayashi,^{3,8} Tatsuya Nagai,¹ Nobuhiko Hamazaki,¹ Aliya Mari D. Adefuin,¹ Fumihiro Miura,⁴ Takashi Ito,⁴ Hiroshi Kimura,⁵ Katsuhiko Shirahige,⁶ Tadayuki Takeda,⁷ Katsunori Iwasaki,² Takuya Imamura,¹ and Kinichi Nakashima^{1,9,*}

¹Department of Stem Cell Biology and Medicine, Graduate School of Medical Sciences, Kyushu University, Fukuoka, Japan

²Department of Neuropharmacology, Faculty of Pharmaceutical Sciences, Fukuoka University, Fukuoka, Japan

³Department of Aging Science and Pharmacology, Faculty of Dental Science, Kyushu University, Fukuoka, Japan

⁴Department of Biochemistry, Graduate School of Medical Sciences, Kyushu University, Fukuoka, Japan

⁵Cell Biology Unit, Institute of Innovative Research, Tokyo Institute of Technology, Tokyo, Japan

⁶Laboratory of Genome Structure and Function, Research Center for Epigenetic Disease, Institute of Molecular and Cellular Biosciences, The University of Tokyo, Tokyo, Japan

⁷Genome Network Analysis Support Facility (GeNAS), RIKEN Center for Life Science Technologies, Kanagawa, Japan

⁸These authors contributed equally

⁹Lead Contact

*Correspondence: tmatsuda@scb.med.kyushu-u.ac.jp (T.M.), kin1@scb.med.kyushu-u.ac.jp (K.N.)

<https://doi.org/10.1016/j.neuron.2018.12.010>

SUMMARY

Minimal sets of transcription factors can directly reprogram somatic cells into neurons. However, epigenetic remodeling during neuronal reprogramming has not been well reconciled with transcriptional regulation. Here we show that NeuroD1 achieves direct neuronal conversion from mouse microglia both *in vitro* and *in vivo*. Exogenous NeuroD1 initially occupies closed chromatin regions associated with bivalent trimethylation of histone H3 at lysine 4 (H3K4me3) and H3K27me3 marks in microglia to induce neuronal gene expression. These regions are resolved to a monovalent H3K4me3 mark at later stages of reprogramming to establish the neuronal identity. Furthermore, the transcriptional repressors *Scrt1* and *Mels2* are induced as NeuroD1 target genes, resulting in a decrease in the expression of microglial genes. In parallel, the microglial epigenetic signature in promoter and enhancer regions is erased. These findings reveal NeuroD1 pioneering activity accompanied by global epigenetic remodeling for two sequential events: onset of neuronal property acquisition and loss of the microglial identity during reprogramming.

INTRODUCTION

Lineage-specific transcription factors enable the switch from one cell type into another, with potential applications in disease modeling and regenerative therapy (Takahashi and Yamanaka, 2006). Mouse fibroblasts, for example, have been converted to

neurons *in vitro* by forced expression of the transcription factors Ascl1, Brn2, and Myt1l (Vierbuchen et al., 2010). In addition to these factors, a neurogenic basic-helix-loop-helix (bHLH) transcription factor, NeuroD1 (ND1), further enhanced the efficiency of direct neuronal conversion from human fibroblasts (Pang et al., 2011). Cultured mouse astrocytes have also been converted to neurons with a single transcription factor, such as ND1 or Neurog2 (Berninger et al., 2007; Guo et al., 2014; Heinrich et al., 2010). More recent studies indicate that exogenous Sox2 or ND1 expression converts endogenous astrocytes in the mouse brain and spinal cord to neurons (Brulet et al., 2017; Guo et al., 2014; Niu et al., 2013, 2015; Su et al., 2014; Wang et al., 2016). Because glial cells, including astrocytes, proliferate in response to injury in the CNS and eventually form a glial scar (Sofroniew, 2009), *in vivo* neuronal conversion from astrocytes raises the possibility of modifying gliotic tissues to provide a cellular source for replenishing impaired neuronal circuits. Microglia, the major immune cells in the CNS, also converge at injured sites and become a predominant cell type within the glial scar (Annunziato et al., 2013; Cregg et al., 2014). Furthermore, a recent report has shown that, even after selective elimination of most microglia (>99%) in the adult mouse brain, the population can be rapidly replenished from the few surviving microglia (<1%) (Huang et al., 2018). Thus, microglia that have accumulated at injured sites should be suitable for restoring lost neurons by direct conversion without exhaustion of the source in the brain. Nevertheless, direct conversion of microglia into neurons has not been achieved.

Epigenetic gene regulation, including DNA methylation and histone modifications, modulates chromatin structure and determines the accessibility of target sites to their transcription factors (Goldberg et al., 2007). Therefore, epigenetic remodeling at cell type-specific gene loci is an important process for the reprogramming of cells. Pioneer factors are defined as a specific class of proteins that penetrate closed chromatin to create accessible



binding sites for other proteins, including general transcription factors (Cirillo et al., 2002; Zaret and Carroll, 2011). During neuronal reprogramming from somatic cells, the pioneer transcription factor Ascl1 occupies closed chromatin and, consequently, enhances neuronal gene expression in the initial phase of reprogramming (Wapinski et al., 2013). Moreover, the pioneering activity is promoted by small molecules such as forskolin and dorsomorphin in the case of Neurog2-mediated neuronal conversion (Smith et al., 2016). Although accumulating studies have provided mechanistic explanations for pioneer factor-mediated induction of specific gene expression in reprogrammed neurons, it remains largely unclear how these factors can simultaneously silence genes that were expressed in the original cells during and/or after neuronal conversion.

Here we report that a single transcription factor, ND1, can directly convert mouse microglia into neurons. ND1-converted neurons express mature neuronal markers and form synaptic networks with primary cultured cortical neurons. To provide mechanistic insights into this conversion, we performed chromatin immunoprecipitation followed by sequencing (ChIP-seq) for ND1 and four histone marks (H3K4me1, trimethylation of histone H3 at lysine 4 [H3K4me3], H3K27me3, and H3K27ac), whole-genome bisulfite sequencing (WGBS), and RNA sequencing (RNA-seq). We found that ND1 penetrated closed chromatin associated with bivalent modifications (H3K4me3 and H3K27me3) to initiate expression of neuronal genes and, consequently, remodeled the chromatin landscape from the bivalent to the monovalent state (H3K4me3). We also observed that the expression of *Brn2*, a gene directly induced by ND1, supports acquisition of the neuronal gene expression pattern, whereas expression of other ND1 target genes (*Scrt1* and *Meis2*) represses microglial gene expression through the reduction of transcription factors, including Lyl1 and Mafb, which are important for the development and maintenance of immune cells (Bakri et al., 2005; Zohren et al., 2012). In parallel, ND1 reorganized global DNA methylation and histone modification patterns in microglial promoter and enhancer regions, most likely to suppress microglial identity. These results suggest that ND1 triggers transcriptional and epigenetic changes in microglia as a pioneer factor to confer neuronal identity and erase microglial identity, respectively. Importantly, we indicate that ND1 can convert microglia to striatal projection neuron-like cells in the adult mouse striatum, shedding new light on the development of therapeutic strategies for CNS injury.

RESULTS

Direct Conversion of Microglia into Neurons

To assess whether microglia can be converted into neurons, we first prepared and cultured CD11b-, CD68-, and Iba1-positive microglia *in vitro* and confirmed that they did not contain β III-tubulin-positive neurons, Nestin-positive neural stem and precursor cells (NS/PCs), glial fibrillary acidic protein (GFAP)-positive astrocytes, or Olig2-positive oligodendrocyte precursor cells, indicating that they were highly enriched microglia (Figures S1A and S1B). We selected eight transcription factors (Ascl1, Brn2, Myt1l, Olig2, Zic1, Sox2, Neurog2, and ND1), one microRNA (*miR124*), and one epigenetic factor (MBD3) as candi-

dates based on their known roles in reprogramming (Ambasudhan et al., 2011; Brulet et al., 2017; Heinrich et al., 2010; Niu et al., 2013; Pang et al., 2011; Rais et al., 2013; Vierbuchen et al., 2010). We used lentiviruses encoding each of these factors or short hairpin RNA (shRNA) for MBD3 and expressed them under the control of the doxycycline (Dox)-inducible tetracycline response element (TRE) promoter (Figures 1A and S1C). Among these factors, ND1 overexpression showed the highest induction of β III-tubulin-positive cells 6 or 7 days post Dox treatment (dpt) (Figures 1B, S1D, and S1E), although the expression of exogenous ND1 was almost extinguished by 7 dpt (Figure S1F). We found that 35% and 25% of ND1-transduced microglia had become β III-tubulin-positive and Map2ab-positive and β III-tubulin-negative cells at 7 dpt, respectively, whereas only 13% were Iba1-positive (Figures S1G and S1H). Comparable amounts of neuronal marker-positive cells were observed in ND1-transduced microglia that had been activated by stimulation with lipopolysaccharide (LPS) (Figure S1J).

To confirm this conversion, we expressed a reverse tetracycline-controlled transactivator (rtTA) under the *Iba1* promoter, allowing restricted expression of TRE-controlled genes in microglia (Figure S2A). Using this system, we detected β III-tubulin-, doublecortin (DCX)- and Map2ab-positive cells bearing a neuron-like morphology in ND1-transduced microglia (Figure S2B). Because the human *CD68* promoter has been reported to enable immune cell-specific transgene expression in the mouse (Iqbal et al., 2014), and *CD68* is specifically expressed in microglia in the brain, we employed this promoter to further investigate the microglia-neuron conversion. We observed *ND1* expression under control of the human *CD68* promoter and neuronal marker-positive cells in the transduced microglia (Figures S2C and S2D), indicating that ND1 can indeed convert microglia to induced neuronal (iN) cells. Next, we sought to determine whether this conversion passes through an NS/PC state. To this end, we cultured microglia with 5-ethynil-2'-deoxyuridine (EdU) throughout the conversion period (Figure S2E). Five days after the onset of EdU treatment, the majority of the neuronally converted cells were EdU-negative (Figures S2F and S2G). In addition, qRT-PCR analysis revealed ND1-enhanced mRNA expression of neuronal genes such as *Dcx* and *Tubb3*, whereas no change was observed in the expression of NS/PC-related genes (*Sox2*, *Pax6*, and *Nestin*) (Figure S2H), suggesting that ND1 converts microglia directly into iN cells with no intermediate NS/PC state. To examine whether these iN cells are glutamatergic or GABAergic, we performed immunostaining with antibodies for VGLUT1 and GAD67 and found that 74.2% of iN cells were positive for VGLUT1 at 21 dpt, whereas 25.7% were stained for GAD67 (Figures S2I and S2J).

To explore whether these converted neurons integrate into existing neuronal circuits *in vitro*, microglia were labeled with tdTomato and converted to iN cells under co-culture with primary cultured neurons (Figures S3A–S3C). We found that these fluorescently labeled cells expressed the neuronal marker Map2 together with the mature neuronal marker NeuN and formed excitatory synapses with tdTomato-negative primary cultured neurons (Figures S3D and S3E). Furthermore, calcium imaging revealed neuronal activity in iN cells in response to N-methyl-D-aspartate (NMDA) stimulation, similar to primary cultured

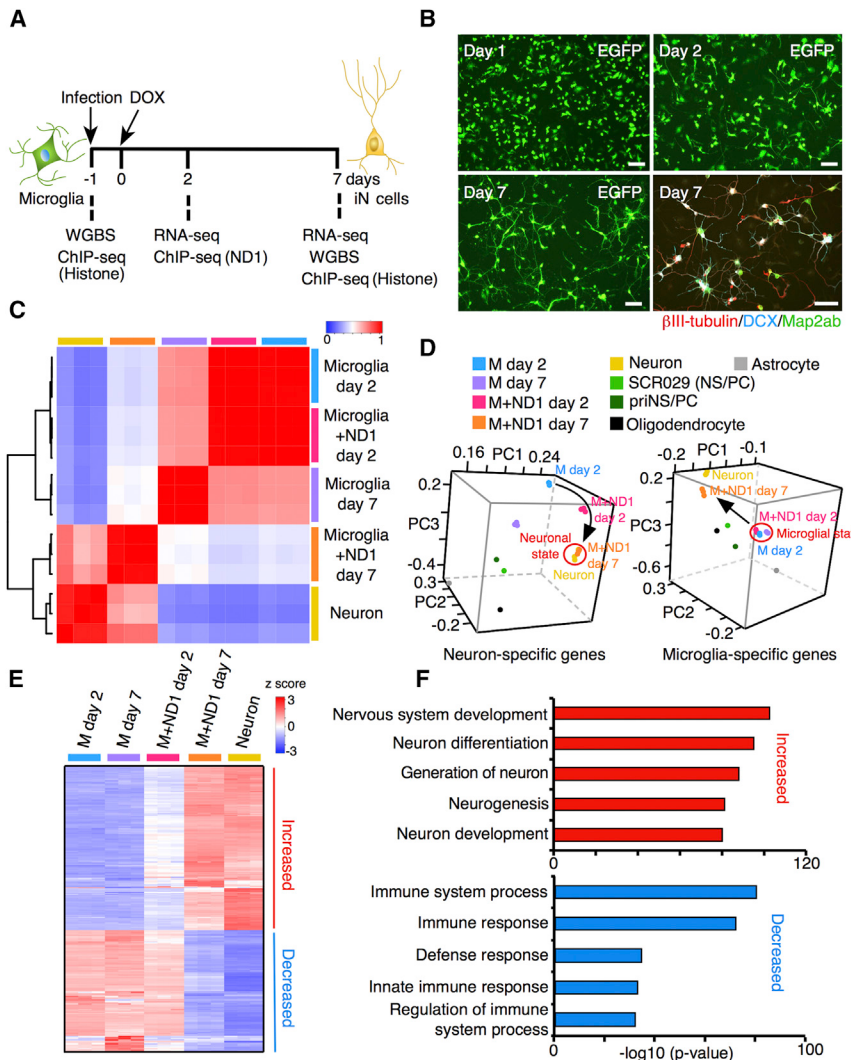


Figure 1. ND1 Induces Global Transcriptional Alterations during Microglia-Neuron Conversion

(A) Schematic representation of the overall experimental design of this study. Microglia infected with lentivirus encoding M2rtTA were used as a control. (B) Representative images of morphological changes of EGFP-positive microglia transduced with ND1. The neuronal markers $\beta\text{III-tubulin}$ (red), Map2ab (green), and DCX (cyan) were expressed in these cells on day 7 (bottom right). See also Figures S1–S3.

(C) Pairwise similarity (Pearson's correlation) between each sample with respect to gene expression and the hierarchical tree resulting from clustering of gene expression (left).

(D) PCA of neuron-specific genes (left, $n = 1,049$) and microglia-specific genes (right, $n = 1,244$) of each sample; microglia day 2 (M day 2), microglia day 7 (M day 7), microglia+ND1 day 2 (M+ND1 day 2), microglia+ND1 day 7 (M+ND1 day 7), neurons, SCR029 cells (NS/PCs), primary cultured NS/PCs (priNS/PCs), oligodendrocytes, and astrocytes. The arrows emphasize the progression of conversion. See also Figure S3.

(E) Heatmap of genome-wide expression analysis during the iN cell reprogramming process by RNA-seq across the indicated time points ($n = 3$ biological replicates). Shown are the 4,325 genes whose expression changed significantly at least 8-fold in ND1-transduced cells (M+ND1 day 7) compared with control microglia (M day 7).

(F) Functional annotation of increased and decreased genes in (E). The top five gene ontology (GO) terms in each gene group are displayed.

ND1 Induces Global Transcriptional Changes in Microglia

To gain deeper insight into how ND1 achieves neuronal conversion from microglia, we analyzed the transcriptome of ND1-transduced microglial cultures

neurons (Figures S3F–S3H), suggesting that these iN cells are functional neuron-like cells with the capacity to integrate into existing neuronal circuits. We next performed patch-clamp recordings of iN cells and observed spontaneous action potential firing in iN cells under the current clamp condition (Figure S3I). To ensure that these firing responses were indeed action potentials, a depolarization stimulus was given to the soma from the patch pipette, and action potentials could be elicited by depolarizing the membrane (Figure S3J); these were completely blocked by tetrodotoxin (TTX) (Figure S3K), a specific inhibitor of Na^+ ion channels. iN cells also exhibited properties similar to neurons in terms of membrane capacity, resting membrane potential, and input resistance (Figures S3L–S3N). Moreover, we recorded spontaneous synaptic currents under the voltage-clamp condition at a holding potential of -70 mV and observed them constantly (Figures S3O, S3P, and S3Q). These results indicated that iN cells had been functionally converted to neurons capable of generating action potentials and spontaneous synaptic currents.

with a high infection rate (>97%) at 2 and 7 dpt (Figures 1A, 1B, S3Q, and S3R) and observed a high correlation ($r > 0.98$, Pearson's correlation) between biological replicates (Figure 1C). Notably, global gene expression in ND1-transduced cells at 7 dpt resembles that in primary cultured neurons (Figure 1C). To ascertain whether ND1 indeed altered cell identity, we then performed principal-component analysis (PCA). The results indicated that the expression pattern of neuron-specific genes in ND1-transduced cells at 7 dpt is very similar to that in primary cultured neurons, whereas the pattern of microglia-specific genes in these converted cells is distinct from microglia (Figure 1D), suggesting that forced expression of ND1 provokes and suppresses neuronal and microglial programs, respectively. Furthermore, the expression pattern of neural stem cell (NSC)-specific genes in ND1-transduced cells at 2 and 7 dpt was distinct from that of NSCs (Figure S3S), further supporting our conclusion that ND1 converts microglia directly into iN cells without their passing through an NS/PC state (Figures S2F–S2H). To substantiate these conclusions, we identified genes

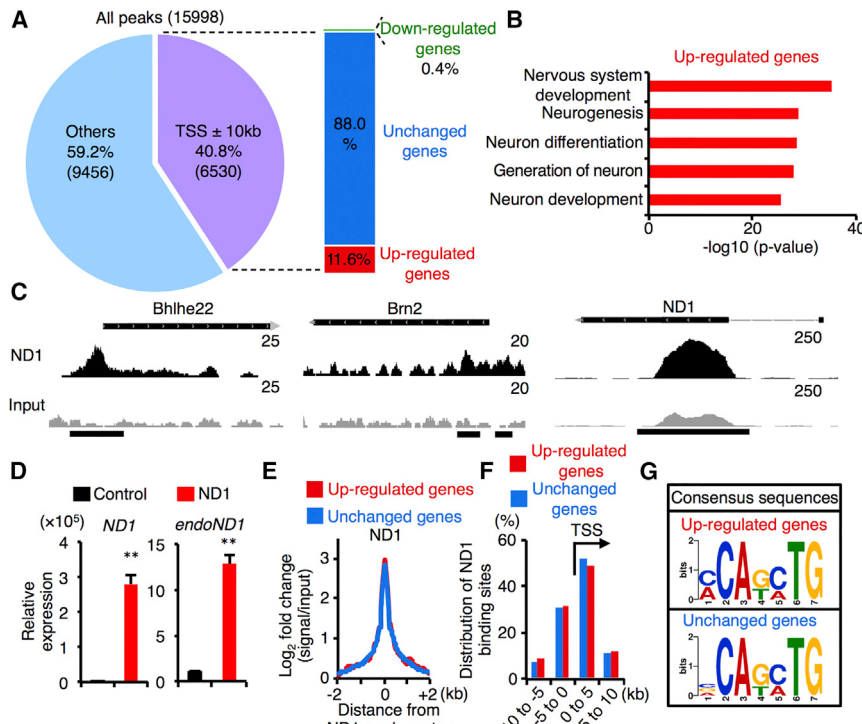


Figure 2. ND1 Binds to Neuronal Gene Loci and Increases Their Expression

(A) Pie chart (left) showing the percentage of ND1 peaks within 10 kb up- or downstream of a TSS. These ND1-bound genes were classified into three groups (right) based on their expression changes in ND1-transduced microglia at 2 dpt relative to the control: downregulated (fold change ≤ 0.5 , $q < 0.05$ by a program in Cufflinks), upregulated (fold change ≥ 2 , $q < 0.05$ by a program in Cufflinks), and unchanged (others) genes.

(B) Functional annotation of upregulated genes in (A). The top five GO terms are displayed.

(C) Alignment of ND1 ChIP-seq (black) and input (gray) data near the *Bhlhe22*, *Brn2*, and *ND1* loci. Black lines at the bottom show the model-based analysis of ChIP-seq (MACS)-annotated regions for ND1 binding.

(D) qRT-PCR analyses of total (left) and endogenous (right) *ND1* levels in ND1-transduced microglia at 2 dpt ($n = 3$ biological replicates). ** $p < 0.01$ by Student's t test.

(E) Enrichment profile at ND1-bound sites (± 2 kb) for ND1 located around upregulated (red) and unchanged (blue) genes.

(F) Distribution of ND1-binding loci around upregulated (red) and unchanged (blue) genes relative to TSS position.

(G) Motif enrichment analysis against ND1-bound sites (± 100 bp) around upregulated (top) and unchanged (bottom) genes. The most enriched motif in each group is displayed. Both groups show similar E-box sequences (CANNTG).

whose expression was either increased ($n = 2,612$) or decreased ($n = 1,724$) in ND1-transduced cells at 7 dpt relative to microglia transduced with the M2rtTA-expressing virus alone (fold change ≥ 8 , $q < 0.05$) (Figure 1E). These genes were subjected to gene ontology analysis of biological processes, which showed that genes induced by ND1 are associated with neuronal development and differentiation (Figure 1F). ND1-suppressed genes, on the other hand, were enriched in processes associated with immune responses (Figure 1F). Interestingly, it seems that the acquisition of neuronal characteristics had already commenced in ND1-transduced cells at 2 dpt, whereas the loss of microglial properties had barely started by this early time point (Figures 1D and 1E). These data suggest that ND1 drives activation of the neuronal program prior to suppression of the microglial program during the conversion.

ND1 Directly Binds Regulatory Elements of Neuronal Genes

To find initial targets of ND1 binding, we performed ChIP-seq for ND1 in microglia at 2 dpt, when extensive changes in neuronal gene expression had already been observed (Figures 1D and 1E), and identified 15,998 significantly ND1-occupied loci using input DNA as a control (Figure 2A). Approximately 41% of them were annotated within 10 kb from the transcription start site (TSS) of a gene, and 11.6% of such annotated loci neighbored significantly upregulated genes (fold change ≥ 2 , $q < 0.05$) in ND1-transduced microglia at 2 dpt relative to microglia (Figure 2A). These ND1-occupied and upregulated genes

(hereafter referred to as upregulated genes) were neuronal development- and differentiation-associated genes, such as *Bhlhe22* (also known as *Bhlhb5*) and *Brn2* (Figures 2B and 2C), suggesting that ND1 directly increases the expression of many of these neuronal genes. Furthermore, exogenous ND1 binds to the endogenous *ND1* locus (Figure 2C) and induces its own expression, similar to other self-regulatory reprogramming factors, including Neurog2 (Figure 2D; Liu et al., 2013). Interestingly, the expression of genes neighboring 88% of ND1-occupied loci located around a TSS was unchanged (hereafter referred to as unchanged genes) (Figure 2A), even though no significant difference between upregulated and unchanged genes was detected regarding ND1 enrichment, distribution around genes, or the identified consensus sequences of ND1-bound regions (Figures 2E–2G).

ND1 Preferentially Binds Unmethylated CpG-Rich Regions

To look more closely at ND1 activity around upregulated and unchanged gene loci, we decided to focus on epigenetic modifications, such as DNA methylation and histone modifications. Samples collected from cultured microglial cells before ND1 transduction were subjected to ChIP-seq (H3K4me1, H3K4me3, H3K27ac, and H3K27me3) and WGBS, which enabled us to explore signatures of pre-existing histones and DNA methylation marks in the original microglia (Figure 1A). We first analyzed the WGBS data and observed that methylation levels around actual ND1 binding sites in microglia are quite low

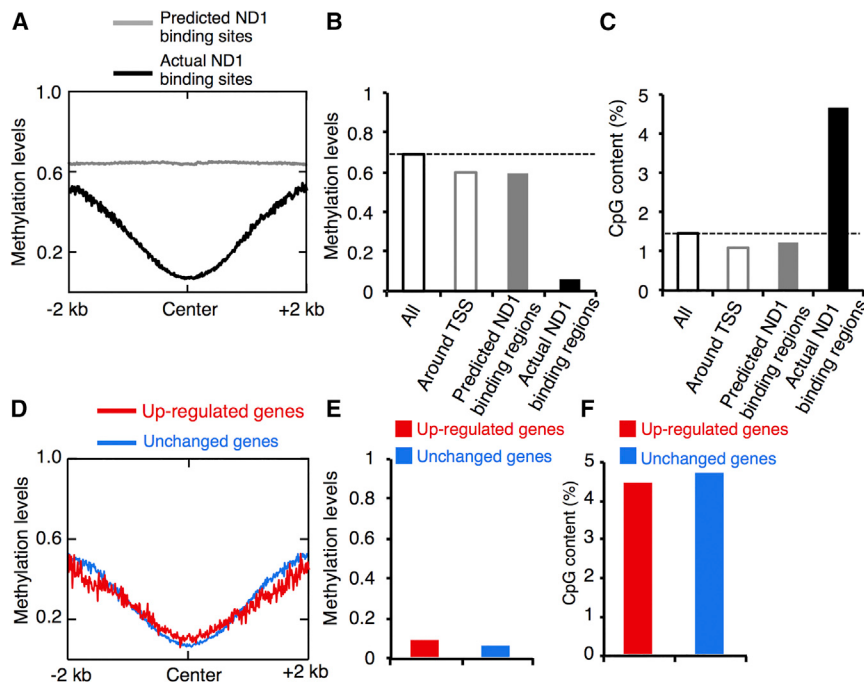


Figure 3. WGBS Reveals Preferential Binding of ND1 to Unmethylated CpG-Rich Regions

(A) Distribution of DNA methylation levels within 2 kb upstream or downstream of actual (green, $n = 6,530$) and predicted (gray, $n = 1,034,549$) ND1 binding sites. Predicted ND1 binding sites were identified based on the known ND1 binding motif sequence (CAGCTG) within the whole genome.

(B) Average DNA methylation levels in all CpG sites, CpG sites around TSSs (± 10 kb), and CpG sites within predicted or actual ND1 binding regions (ND1 binding sites ± 100 bp) located around TSSs (± 10 kb).

(C) CpG content in the whole genome, TSSs (± 10 kb), and predicted or actual ND1 binding regions (ND1 binding sites ± 100 bp) located around TSSs (± 10 kb).

(D) Distribution of DNA methylation levels around the actual ND1 binding sites (± 2 kb) occupied in upregulated (red, $n = 764$) and unchanged genes (blue, $n = 5,735$).

(E) Average DNA methylation levels in CpG sites within the actual ND1 binding regions (ND1 binding sites ± 100 bp) in upregulated (red) and unchanged (blue) genes.

(F) CpG content in the actual ND1 binding regions (ND1 binding sites ± 100 bp) in upregulated (red) and unchanged (blue) genes.

compared with those around ND1 binding sites predicted by the known ND1 binding motif (CAGCTG) (Figures 2G, 3A, and 3B). Moreover, the CpG content was higher in regions around actual ND1 binding sites than in regions around predicted ND1 binding sites (Figure 3C). These data indicate that ND1 preferentially binds unmethylated CpG-rich regions. However, we did not detect any differences in any of these analyses between upregulated and unchanged genes (Figures 3D–3F). Taken together, these data suggest that DNA methylation affects ND1 binding to the genome but is unlikely to contribute to the subsequent gene expression.

ND1 Occupies Bivalent Domains and Induces Neuronal Reprogramming

We then asked whether histone modifications affect ND1 activity. The intensity of pre-existing histone marks in microglia indicated enrichment of active marks (H3K4me3 and H3K27ac) at ND1-bound sites around unchanged genes (Figure 4A). In contrast, enrichment of both active and repressive marks (H3K4me3 and H3K27me3, respectively), a configuration described as a bivalent domain, was observed at ND1-bound sites around upregulated genes (Figures 4A and S4A–S4C) whose expression was initially silenced in microglia (Figure S4D). We also observed that H3K27me3 accumulates on both sides of the H3K4me3 peak at the ND1-bound sites (Figure 4A and S4A), consistent with previous observations that target regions of TrxG proteins, which methylate H3K4, display a reduced H3K27 methylation status (Papp and Müller, 2006; Srinivasan et al., 2008) because of the fact that active chromatin marks, including H3K4me3, inhibit H3K27me3 modification by PRC2 (Schmitges et al., 2011). Furthermore, we obtained publicly available data of

ATAC-seq (assay for transposase-accessible chromatin with high-throughput sequencing) for microglia (Lavin et al., 2014; Matcovitch-Natan et al., 2016) and applied them to our analyses to determine open or closed chromatin states of ND1-bound sites. The results indicated that ND1-bound sites located around upregulated genes have a relatively closed chromatin status, in accordance with their epigenetic signatures and gene expression levels (Figures 4A, S4D, and S4E). These data indicate that ND1 accesses closed chromatin with bivalent modifications to induce the expression of neuronal development- and differentiation-related genes as a pioneer factor. We also found that unchanged genes associated with active epigenetic signatures were strongly expressed in microglia and exhibited high expression regardless of ND1 binding (Figure 4A and S4D). This is probably because unchanged genes were enriched for genes involved in metabolic processes, which are essential for all types of cells (Figure S4F). Thus, the bivalent signature predicts permissiveness for ND1 binding and subsequent induction of gene expression.

We next asked whether the presence of a bivalent chromatin state could predict ND1-mediated reprogramming in other glial cell lineages, i.e., astrocytes and oligodendrocytes. We first established mouse astrocytes *in vitro* and cultured them without growth factors (Figure S5A), a condition under which they display properties closely resembling those of non-reactive astrocytes in the physiological state (White et al., 2011). In accordance with our earlier findings (Brulet et al., 2017), we observed few Map2ab-positive cells in ND1-transduced non-reactive astrocytes at 7 dpt (Figures S5B and S5C). This result is in marked contrast to a previous study in which astrocytes were grown in the presence of epidermal growth factor (EGF) and fibroblast

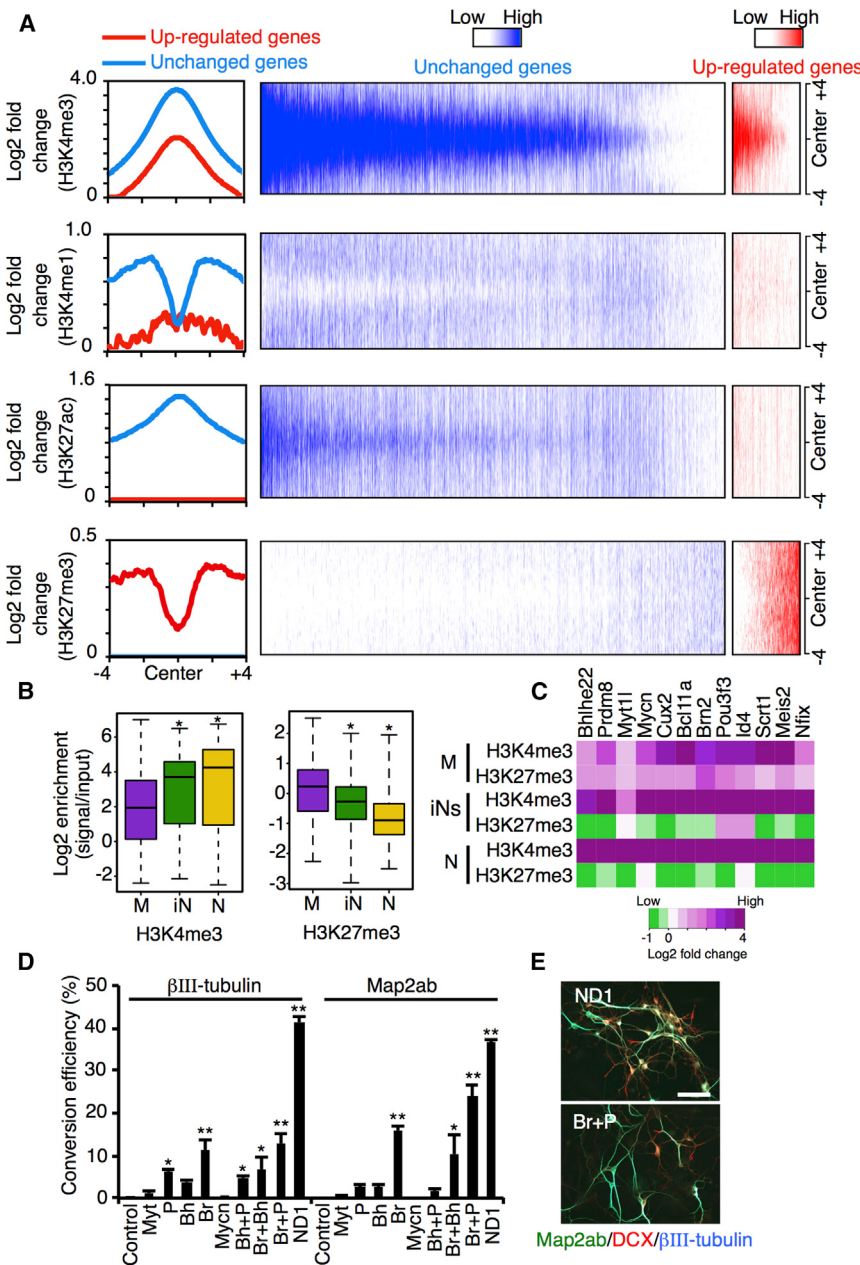


Figure 4. ND1 Occupies Bivalent Domains to Induce Neuronal Gene Expression

(A) Enrichment profile and heatmap of H3K4me3, H3K4me1, H3K27ac, and H3K27me3 around ND1 binding peaks (± 4 kb) located near upregulated (red) and unchanged (blue) genes. See also Figures S4 and S5 and Table S1.

(B) Enrichment of H3K4me3 (left) and H3K27me3 (right) around ND1 binding peaks (± 100 bp) located near upregulated genes in microglia (M), ND1-transduced microglia at 7 dpt (iN), and neurons (N). * $p < 2.2 \times 10^{-16}$ by Wilcoxon rank-sum test.

(C) Heatmap showing the enrichment of H3K4me3 and H3K27me3 around ND1 binding peaks (± 100 bp) located near 12 potential ND1 target genes in microglia (M), ND1-transduced microglia at 7 dpt (iN), and neurons (N).

(D) Quantification (D) and representative images (E) of βIII-tubulin and Map2ab-positive cells in microglia 7 days after overexpression of the indicated ND1 target genes: *Myt1l* (Myt), *Prdm8* (P), *Bhlhe22* (Bh), *Brn2* (Br), and *Mycn* (Mycn). * $p < 0.05$ and ** $p < 0.01$ by ANOVA with Tukey post hoc tests compared with the control.

neuronal conversion of these cells. These results provide strong support for the importance of the bivalent chromatin state in ND1-mediated reprogramming.

Although the ND1 expression level became lower in microglia in the later phase of conversion (Figure S4G), the expression levels of upregulated genes continued to increase (Figure S4D), leading us to hypothesize that epigenetic reprogramming supports the enhancement of gene expression in the neuronal program. To test this, we performed ChIP-seq analysis for H3K27me3 and H3K4me3 in ND1-transduced microglia at 7 dpt (iN cells) and in primary cultured neurons (Figure 1A). We observed an increase in H3K4me3 levels in the ND1-bound regions around upregulated genes in iN cells compared with microglia (Figures 4B, 4C, and S4A). In contrast, the

growth factor 2 (FGF2) (Guo et al., 2014). EGF and FGF2 are known to be upregulated in reactive astrocytes in response to injury, and they probably confer a more “stem-like” property on astrocytes (Robel et al., 2011). Oligodendrocytes, on the other hand, were converted into Map2ab and NeuN-positive cells 7 days after ND1 transduction (Figures S5D–S5I). By performing ChIP-qPCR analysis in non-reactive astrocytes and oligodendrocytes, we next assessed histone modifications of neuronal genes (*Bhlhe22*, *Prdm8*, *Brn2*, and *Pou3f3*), which have been shown to have the bivalent signature (H3K4me3 and H3K27me3) in microglia. As shown in Figures S5J and S5K, we found that the bivalent signature was enriched in these genes in oligodendrocytes but not astrocytes, in accordance with the capacity of ND1 to induce

levels of H3K27me3 in these regions decreased significantly during conversion. However, although they are morphologically and functionally similar (Figures S3B–S3P), the extent of these histone modifications in iN cells did not reach their extent in primary cultured neurons (Figures 4B and 4C), perhaps because iN cells may require additional time to gain the same epigenetic profile possessed by neurons or because iN cells may not have an epigenetic profile identical to that of neurons, as observed in the case between induced pluripotent stem cells (iPSCs) and embryonic stem cells (Ma et al., 2014).

To investigate how ND1 expression alters the epigenome, we identified differentially expressed genes associated with function in epigenetic modification and chromatin remodeling ($n = 171$)

whose expression levels were significantly changed by ND1 transduction in microglia at 2 dpt ($n = 20$, $q < 0.05$, fold change ≥ 1.5) and 7 dpt ($n = 87$, $q < 0.05$, fold change ≥ 1.5) (Table S1; Figure S5L). Among them, we found that ND1 bound to the region around the TSS of *Jmjd3*, a histone H3K27 demethylase gene, and upregulated its expression (Figures S5M and S5N), suggesting that ND1 resolves bivalent domains to a monovalently marked state during neuronal reprogramming, at least in part because of the direct induction of *Jmjd3* expression.

Integrative analysis of our transcriptional and epigenetic data identified 20 transcription factor genes bearing bivalent domains as potential ND1 target genes, which might mediate the iN cell reprogramming process (Table S2). A literature survey revealed that 14 of these 20 factors potentially play important roles in the generation and maintenance of neurons (Table S2). Among these candidates, we selected the top four upregulated transcription factors (*Bhlhe22*, *Prdm8*, *Myt1l*, and *Mycn*) in addition to one (*Brn2*) that is known to induce neuronal reprogramming. With the exception of *Mycn*, individual expression of these genes could induce neuron-like cells (Figures 4D and 4E). Combinatorial expression of two genes, *Brn2* and *Prdm8*, further enhanced the conversion from microglia to neuron-like cells (Figures 4D and 4E). We also found that combinatorial expression of *ND1* and *Brn2* increased the efficiency of reprogramming mediated by *ND1* alone (Figure S5O and S5P). In contrast, when we reduced the expression of *Brn2* by shRNAs (sh1 and sh2), the efficiency of *ND1*-mediated reprogramming was decreased (Figure S5Q–S5S). These results suggest that *Brn2* acts as an essential *ND1* target gene to induce neuronal reprogramming.

Suppression of Microglia-Specific Gene Expression Is Mediated in Part by Direct *ND1* Target Genes

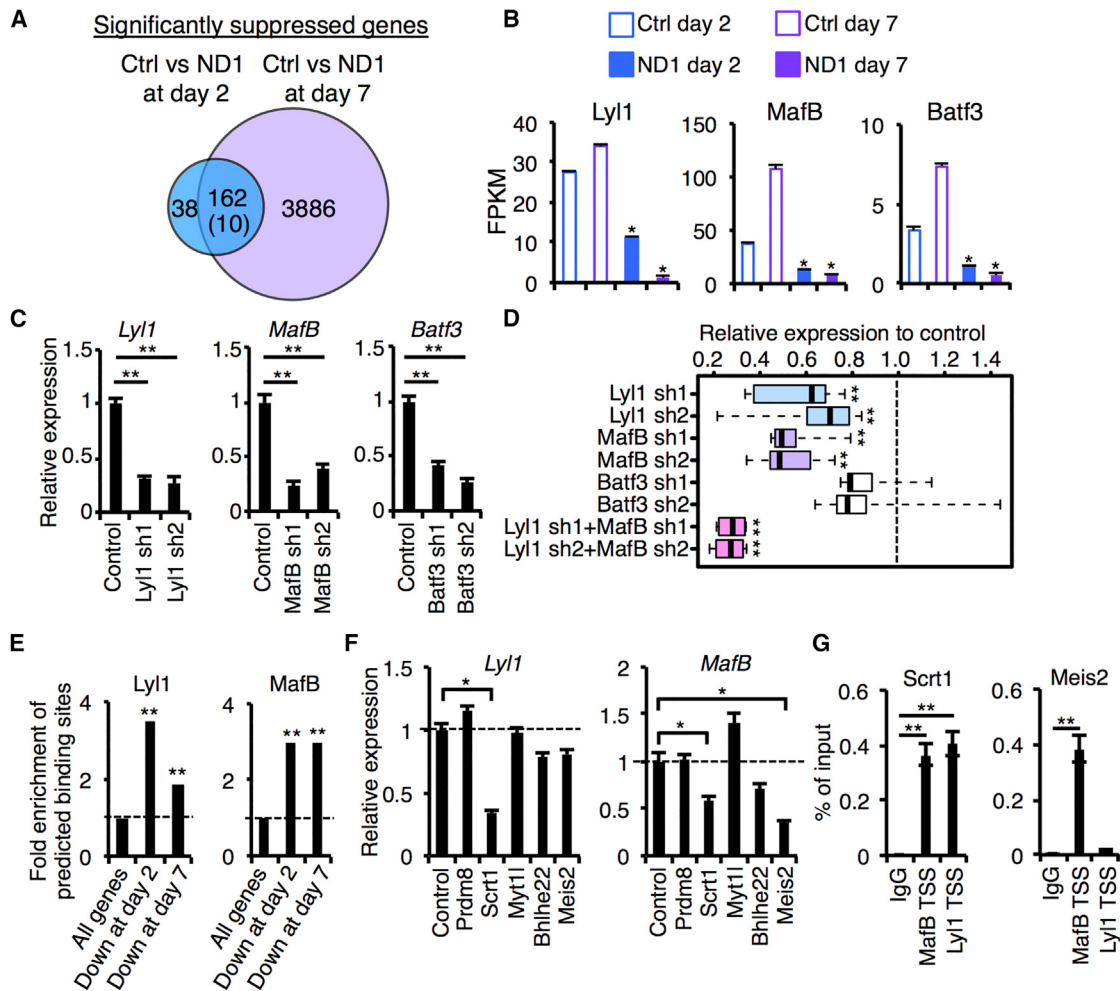
Microglial identity was attenuated during iN cell reprogramming through the reduction of immune gene expression (Figures 1D–1F). Therefore, we next investigated how *ND1* expression accomplishes transcriptional repression of immune genes in microglia. We identified genes persistently downregulated in *ND1*-transduced cells at 2 dpt and 7 dpt ($n = 162$) relative to control microglia (fold change ≤ 0.5 , $q < 0.05$) (Figure 5A), and these genes included 10 transcription factors. A literature survey further revealed that four of the 10 transcription factors potentially play important roles in development and differentiation of immune cells (Table S3). Among these four factors, we selected the top three silenced transcription factors (Figure 5B) and designed two distinct shRNAs (sh1 and sh2) for each. Infection of the microglial cell line BV2 with lentiviruses harboring these shRNAs decreased the expression of the candidate factors (Figure 5C). In addition, we found that *Mafb* and *Lyl1*, but not *Batf3* knockdown, resulted in a significant reduction in the expression of immune genes, including *Ccl3*, *Ccl4*, *Cebpa*, *Irf8*, *Pu.1*, and *p65* in microglia (Figure 5D and S6A), and combinatorial knockdown of *Mafb* and *Lyl1* caused a further decrease in expression (Figures 5D and S6A). To check whether *Lyl1* and *Mafb* could regulate the expression of other immune genes, we analyzed public ChIP-seq data for these transcription factors (Schütte et al., 2016; Soucie et al., 2016) and found that they potentially bind to the pro-

moters of silenced genes at both 2 dpt and 7 dpt (Figure 5E), including many microglia-specific genes associated with immune functions (Figure S6B). These data suggest that *Mafb* and *Lyl1* regulate microglial cell identity through the maintenance of microglial gene expression.

Because *ND1* transduction decreased *Mafb* and *Lyl1* expression in microglia even though *ND1* is a known transcriptional activator (Figure 2A), we next investigated whether *ND1* induces transcriptional repressors, which subsequently suppress *Mafb* and *Lyl1* expression. We individually expressed five transcriptional repressors among 14 *ND1* target genes known to play important roles in the generation and maintenance of neurons (Table S2) in microglia and found that *Scrt1* and *Meis2* bound to the TSS regions of *Mafb* and *Lyl1*, leading to their suppression (Figures 5F and 5G). Although *Myt1l* is an important repressive transcription factor for blocking non-neuronal programs in fibroblasts (Mall et al., 2017), it did not affect the expression of these microglial genes (Figure 5F). Nevertheless, these results suggest that *ND1* initially induces the expression of neuronal genes, including *Scrt1* and *Meis2*, which subsequently suppress the microglial program by silencing *Mafb* and *Lyl1* expression, supporting the idea that *ND1* confers neuronal identity on microglia prior to extinguishing microglial cell identity during reprogramming.

ND1 Induces Epigenetic Reprogramming and Suppresses the Microglial Program

We further investigated whether *ND1* induces epigenetic remodeling around microglia-specific genes to suppress microglial identity during neuronal reprogramming. ChIP-seq analysis revealed a significant increase in H3K27me3 and decrease in H3K4me3 levels in the promoters of microglia-specific genes during neuronal reprogramming, although the extent of histone modification did not reach that seen in neurons (Figure 6A). By comparing DNA methylation patterns in CNS cells (astrocytes, neurons, oligodendrocytes, and microglia), we next identified microglia-specific hypomethylated sites that potentially shape the profile of microglia-specific gene expression (Figure 6B). Approximately 42% of microglia-specific hypomethylated sites were highly methylated (≥ 1.5 -fold) in iN cells compared with microglia (Figure 6C). Furthermore, these hypermethylated sites were highly enriched in active microglial enhancer regions that were co-occupied by H3K4me1 and H3K27ac (Figure 6D). We searched for consensus sequences around the identified hypermethylated sites in iN cells using the algorithm MEME (multiple expectation-maximization [EM] for motif elicitation) (Bailey et al., 2009), and found that multiple immune-related transcription factors, including *Mafb*, were enriched around these sites (Figure 6E). We also obtained public ChIP-seq data for important immune-related factors from macrophages (Kaikkonen et al., 2013; Langlais et al., 2016; Mancino et al., 2015; Menéndez-Gutiérrez et al., 2015; Ng et al., 2011; Ostuni et al., 2013; Soucie et al., 2016), allowing us to assess the enrichment of these factors in hypermethylated sites in iN cells compared with randomly selected CpG sites (Figure 6F). These hypermethylated site-enriched factors include basic leucine zipper domain (bZIP) family (*Mafb*, *Batf3*, *Cebpa*, *Junb*, and *Jdp2*) and heat shock transcription factor (HSF) family (HSF1) proteins that predominantly bind

**Figure 5. ND1 Target Genes Suppress the Microglial Program**

(A) Venn diagrams showing the number of unique or common repressed genes in ND1-transduced microglia at 2 dpt ($n = 200$) and 7 dpt ($n = 4,048$) compared with each control (fold change ≤ 0.5 , $q < 0.05$ by a program in Cufflinks). The 162 common genes include 10 transcription factors.

(B) Bar graphs showing the expression levels of three genes that potentially regulate the microglial program in control and ND1-transduced microglia ($n = 3$ biological replicates). * $p < 0.05$ by a program in Cufflinks.

(C) qRT-PCR analyses of the expression of the three candidate genes in BV2 cells. Each shRNA significantly reduces candidate gene expression ($n = 3$ biological replicates). ** $p < 0.01$ by ANOVA with Tukey post hoc tests.

(D) qRT-PCR analyses of the immune genes silenced in ND1-transduced cells at 7 dpt (*Cebpa*, *Irf8*, *Ccl3*, *Pu.1*, *p65*, and *Ccl4*). Boxplots show the relative expression of these six immune genes in microglia 4 days after each shRNA transduction. *Lyl1* and *Mafb* shRNA significantly reduce the expression of these immune genes, unlike *Batf3* shRNA. * $p < 0.05$ and ** $p < 0.01$ by Wilcoxon rank-sum test. See also Figure S6.

(E) Enrichment of predicted *Lyl1* and *Mafb* binding sites in promoter regions (± 2 kb from TSSs) of all genes (left) and silenced genes at the indicated time points (center and right) during conversion. These predicted binding sites are identified using public ChIP-seq data for *Lyl1* and *Mafb*. The dashed line indicates the expected distribution of promoters. ** $p < 0.01$ by hypergeometric distribution.

(F) qRT-PCR analyses of *Lyl1* and *Mafb* expression in microglia 2 days after transduction of the indicated transcription factors ($n = 5$ biological replicates). * $p < 0.05$ by ANOVA with Tukey post hoc tests.

(G) ChIP-qPCR analyses of *Scrt1* and *Meis2* around the TSSs of *Mafb* and *Lyl1*. Anti-FLAG ChIP was carried out using primary cultured microglia expressing FLAG-tagged *Scrt1* and *Meis2* ($n = 4$ biological replicates). ** $p < 0.01$ by ANOVA with Tukey post hoc tests.

to unmethylated CpG-containing sites (Yin et al., 2017). Taken together, these findings suggest that ND1 reprograms the epigenetic landscape, such as histone modifications and DNA methylation, around promoter and enhancer regions to disrupt the binding of immune-related transcription factors, resulting in suppression of microglial cell identity.

ND1 Can Induce Reprogramming from Microglia to Neurons in the Adult Mouse Brain

Because endogenous adult neurogenesis is insufficient for brain repair, *in vivo* neuronal reprogramming from endogenous non-neuronal cells is a promising technology to replenish lost neurons. To test whether ND1 is capable of reprogramming

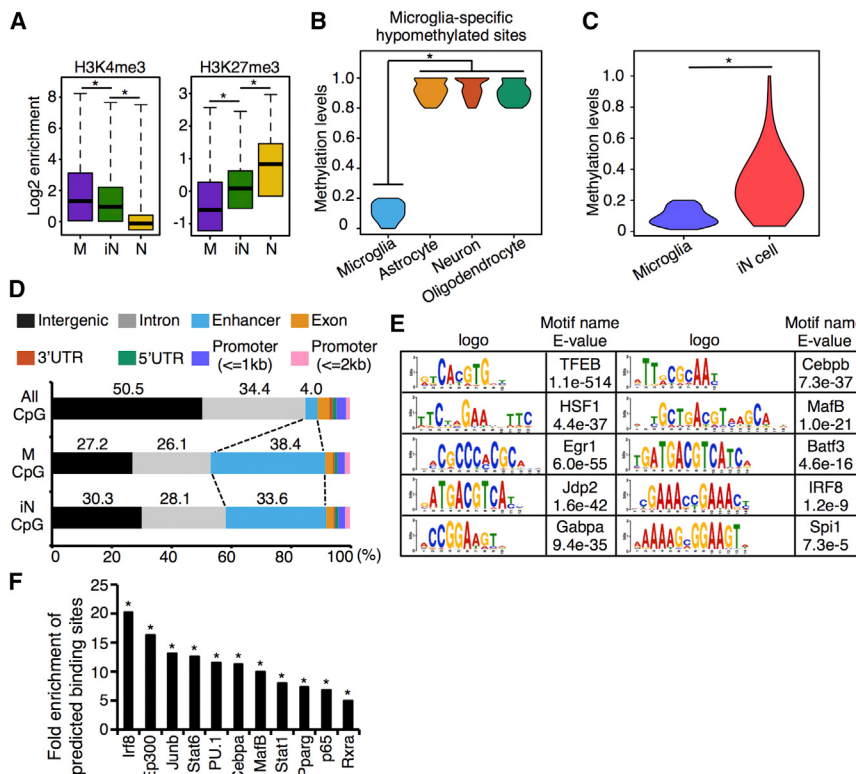


Figure 6. ND1 Induces Epigenetic Remodeling in Microglial Promoter and Enhancer Regions

(A) Enrichment of H3K4me3 (left) and H3K27me3 (right) in microglia (M), ND1-transduced microglia at 7 dpt (iN), and neurons (N) on the promoter regions of microglia-specific genes ($n = 1,244$). * $p < 2.2 \times 10^{-16}$ by Wilcoxon rank-sum test.

(B) DNA methylation levels in microglia-specific hypomethylated CpG sites ($n = 54,969$) in microglia, astrocytes, neurons, and oligodendrocytes. * $p < 2.2 \times 10^{-16}$ by Wilcoxon rank-sum test.

(C) DNA methylation levels in hypermethylated CpG sites in iN cells compared with microglia (≥ 1.5 -fold, $n = 23,371$). * $p < 2.2 \times 10^{-16}$ by Wilcoxon rank-sum test.

(D) Distribution of all CpG sites (All CpG), microglia-specific hypomethylated CpG sites (M CpG, $n = 54,969$), and hypermethylated CpG sites in iN cells (IN CpG, $n = 23,371$) for the indicated genetic regions.

(E) Motif enrichment analysis against hypermethylated CpG sites in iN cells (± 100 bp). Motifs significantly enriched in immune genes are displayed.

(F) Enrichment of predicted binding regions of the indicated transcription-related factors in hypermethylated CpG sites ($n = 23,371$) relative to randomly generated sites ($n = 23,371$). * $p < 0.01$ by hypergeometric distribution.

microglia into neurons in the adult mouse brain, lentiviral expression of ND1-P2A-EGFP under the promoter of human CD68 was employed to explicitly identify ND1-transduced cells using co-expressed EGFP as the marker. When we injected the lentiviruses into the striatum of 8-week-old mice, approximately 60% of the control virus-infected cells expressed Iba1 together with the microglia-specific marker Tmem119 (Bennett et al., 2016) 2 weeks after viral injection, whereas very few ND1-transduced cells expressed these markers, even though almost no change was observed in other cell populations, such as GFAP-positive astrocytes, APC-positive oligodendrocytes, and Olig2-positive oligodendrocyte precursor cells (Figures 7A and 7B). We performed immunostaining with antibodies for neuronal markers and found that 50% and 33% of ND1-transduced cells were positive for β III-tubulin and Map2ab, respectively (Figures 7C and 7D). Furthermore, when we depleted microglia specifically from the brain by treatment with PLX5622 (Figures S7A and S7B), an inhibitor of colony-stimulating factor-1 receptor (Huang et al., 2018), ND1-reprogrammed DCX-positive cells almost completely disappeared (Figures S7C and S7D). To confirm this result, we employed Rosa-yellow fluorescent protein (YFP) reporter mouse and found that the emergence of DCX and YFP dual-positive cells after lentiviral expression of ND1-P2A-Cre under the control of the CD68 promoter was virtually abolished in the microglia-depleted brain (Figures S7E and S7F). Taking these observations together, it is most likely that the majority of original cells converted into iN cells by CD68-ND1-P2A-EGFP lentivirus infection were microglia in the striatum. When assessed at 4 weeks after

CD68-ND1-P2A-EGFP lentivirus injection, 75% of ND1-transduced cells had become positive for DARPP32, a marker for striatal projection neurons (Figures 7E and 7F). These iN cells formed excitatory synapses with host neurons in the striatum (Figure 7G). We also performed patch-clamp recordings of iN cells in the striatum (Figure S7G). We observed spontaneous action potential firing following depolarization under the current-clamp condition 4 weeks after ND1 transduction (Figures S7H and S7I) and detected spontaneous synaptic events, both excitatory and inhibitory, in iN cells (Figures S7J–S7M). These data indicate that ND1 reprograms microglia to striatal projection neuron-like cells in the adult mouse striatum and that these cells are functionally integrated into brain circuits through synaptic connections with other neurons.

DISCUSSION

ND1 has been shown to enable astrocytes to be converted into neurons (Guo et al., 2014), but the mechanisms involved in this ND1-mediated switch have yet to be determined. Although those authors reported that ND1 failed to induce neuronal reprogramming from microglia, probably because of a low infection efficiency of microglia by the retrovirus (Guo et al., 2014), we found here that lentivirus-mediated ND1 expression efficiently induces neuronal reprogramming both *in vitro* and *in vivo*. Our study further provides a comprehensive description of ND1 occupancy at the initial reprogramming stages and of subsequent transcriptional and epigenetic alterations during neuronal reprogramming.

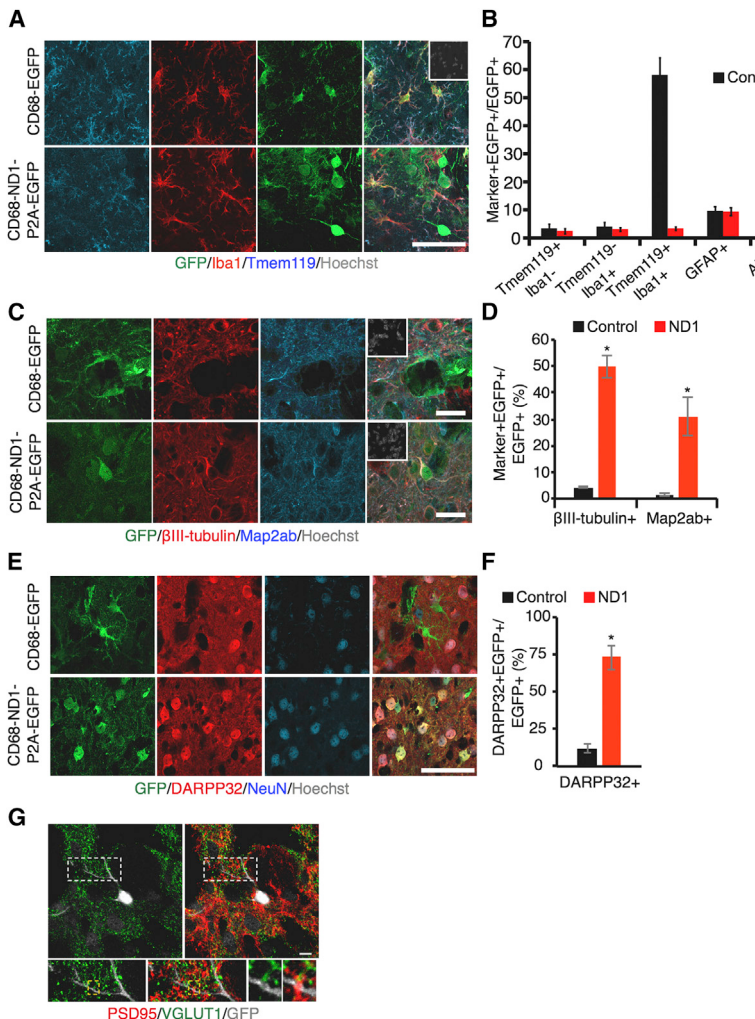


Figure 7. ND1 Executes In Vivo Neuronal Reprogramming from Microglia in the Adult Mouse Striatum

(A) Representative images of staining for EGFP (green), Tmem19 (cyan), and Iba1 (red) in the adult mouse striatum 2 weeks after *in vivo* injection of human CD68 promoter-driven EGFP or ND1-P2A-EGFP lentiviruses. Scale bar, 50 μ m. See also Figure S7.

(B) Quantification of the indicated marker-positive cells in the striatum ($n = 3$).

(C) Representative images of staining for EGFP (green), β III-tubulin (red), and Map2ab (cyan) in the adult mouse striatum 2 weeks after viral injection. Scale bars, 20 μ m.

(D) Quantification of the indicated marker-positive cells in (C) ($n = 3$ animals). * $p \geq 0.05$ by one-tailed Wilcoxon rank-sum test.

(E) Representative images of staining for EGFP (green), DARPP32 (red), and NeuN (cyan) in the adult mouse striatum 4 weeks after viral injection. Scale bars, 50 μ m.

(F) Quantification of DARPP32-positive cells in (E) ($n = 3$ animals). * $p \geq 0.05$ by one-tailed Wilcoxon rank-sum test.

(G) Representative images of staining for GFP, PSD95, and VGLUT1 2 weeks after injection of ND1-P2A-EGFP. The lower images are enlargements of the white or yellow dashed boxes. Scale bar, 10 μ m.

Bivalent genes, characterized by the presence of bivalent domains composed of H3K4me3 and H3K27me3 histone modifications, were initially identified in a subset of key developmentally regulated genes in embryonic stem cells (ESCs) and are thought to prime genes for activation while keeping them repressed (Bernstein et al., 2006; Voigt et al., 2013). As lineage specification progresses, many bivalent domains are resolved to a monovalently marked state (with either H3K4me3 or H3K27me3) (Mikkelsen et al., 2007); however, when assessed in ESC-to-neuron differentiation via NS/PCs, bivalent domains were still observed in neurons because they can be newly formed, even in terminally differentiated cells (Mohn et al., 2008). In the present study, we demonstrated that neuronal genes in the terminally differentiated microglia retained bivalent domains and that the expression of these genes was suppressed (Figures 4A and S4D). ND1 selectively increases the expression of these bivalent genes, although it could bind to H3K4me3-occupied domains regardless of the presence of H3K27me3, suggesting that the bivalent state exists to keep neuronal genes suppressed in microglia and primes these genes for activation at the initial phase of ND1-mediated re-

programming. As neuronal reprogramming proceeded, these bivalent domains resolved to a monovalent H3K4me3 state, and this may have contributed to the cells gaining and maintaining neuronal identity. Thus, it is conceivable that the bivalent domains observed in this study behave during ND1-mediated neuronal reprogramming in a manner similar to how they behave in pluripotent cell differentiation.

A comparison of Ascl1-bound sites during reprogramming of mouse embryonic fibroblasts to neurons and specific histone modifications present at these sites revealed the coexistence of a trivalent chromatin state, composed of two marks associated with an active state (monomethylation of histone H3 at lysine 4 [H3K4me1] and acetylation of histone H3 at lysine 27 [H3K27ac]) and a repressive mark (H3K9me3), on many Ascl1-bound loci (Wapinski et al., 2013). Keratinocytes selected by the absence of such a trivalent state at predicted Ascl1 target sites could not be reprogrammed into neurons following Ascl1 transduction (Wapinski et al., 2013). However, we have shown that ND1, but not Ascl1, can efficiently reprogram microglia to neurons; this is likely because Ascl1 target sites lack such a trivalent state in microglia, although further investigation is warranted. Because ND1 binds to bivalent domains as mentioned above, these findings indicate that the pioneering activity of these two transcription factors relies on distinct patterns of histone modifications at the beginning of reprogramming in the cells.

Suppression of the somatic program has been reported to occur earlier than reactivation of the pluripotency network during reprogramming to iPSCs (Foshay et al., 2012; Koche et al., 2011; Stadtfeld et al., 2008). In support of this, it has been proposed that actively transcribed genes in somatic cells are relatively accessible to reprogramming factors that can silence them, whereas pluripotency-associated genes are rather inaccessible or are occluded by stably bound repressive complexes (Chronis et al., 2017; Foshay et al., 2012). In the present study, we have shown that ND1 invokes the neuronal program before the microglial program is extinguished. ND1 directly induces neuronal genes but indirectly silences microglial genes by directly inducing transcriptional repressor genes such as *Scrt1* and *Meis2*, important factors in brain development (Agoston et al., 2014; Itoh et al., 2013). These findings reveal a stepwise process for the establishment of cell identity during neuronal reprogramming and highlight differences between iPSC and iN cell generation mediated by distinct reprogramming factors.

Reprogramming to iPSCs by transcription factors brings about a global reversion of the somatic epigenome to the pluripotent state for the effective reactivation of pluripotency genes (Chronis et al., 2017; Foshay et al., 2012; Simonsson and Gurdon, 2004). In neuronal reprogramming from fibroblasts, epigenetic regulators such as *Jmjd2d* contribute to this process (Wapinski et al., 2013). In this study, we have shown that forced expression of ND1 in microglia increases H3K27me3 levels and decreases H3K4me3 levels in the promoter regions of microglia-specific genes. Furthermore, ND1 transduction increases DNA methylation levels around enhancer regions for the microglial program. These findings suggest that ND1 instructs reprogramming of the epigenetic landscape to silence microglial cell identity. Because ND1 does not always effectively induce neuronal reprogramming in cells such as non-reactive astrocytes (Brulet et al., 2017), we believe that future studies (e.g., stepwise analysis of the epigenetic profile and chromatin modifier dynamics during neuronal reprogramming from different types of somatic cells) will yield insights into how and when ND1 achieves the rewriting of the epigenetic landscape.

Taken together, our findings provide insights into how a single neurogenic transcription factor, ND1, mediates transcriptional and epigenetic networks during neuronal reprogramming of microglia and bring us one step closer to developing therapeutic strategies for nerve injury and disease by reprogramming microglia that accumulate at lesion sites into neurons.

STAR★METHODS

Detailed methods are provided in the online version of this paper and include the following:

- KEY RESOURCES TABLE
- CONTACT FOR REAGENT AND RESOURCE SHARING
- EXPERIMENTAL MODEL AND SUBJECT DETAILS
 - Mice
 - Primary Cells
 - Cell Lines
- METHOD DETAILS
 - Primary cell isolation and culture

- iN cell induction
- Knockdown experiments
- Immunocytochemistry
- EdU labeling and detection
- Real-time PCR analysis
- Co-culture with primary cultured cortical neurons and calcium imaging
- RNA sequencing and data analysis
- ChIP-seq and data analysis
- WGBS and data analysis
- Microglial ablation
- Stereotactic brain injections
- Immunohistochemistry
- Electrophysiology

- QUANTIFICATION AND STATISTICAL ANALYSIS
- DATA AND SOFTWARE AVAILABILITY

SUPPLEMENTAL INFORMATION

Supplemental Information includes seven figures and four tables and can be found with this article online at <https://doi.org/10.1016/j.neuron.2018.12.010>.

ACKNOWLEDGMENTS

This work was supported by Grant-in-Aid for Research Activity Start-Up 15H06474 (to T.M.), Grant-in-Aid for JSPS Fellows 16J06261 (to T.M.), Grant-in-Aid for Young Scientists (B) 18K14820 (to T.M.), a Hayashi grant-in-aid for basic medical research (Kyushu University) (to K.N.), Grant-in-Aid for Scientific Research on Innovative Areas 16H06527 (to K.N.), and the Platform Project for Supporting Drug Discovery and Life Science Research (Basis for Supporting Innovative Drug Discovery and Life Science Research [BINDS]) from the Japan Agency for Medical Research and Development (AMED) under grants JP16am0101102, JP16am0101103, and JP16am0101105. We thank Dr. K.F. Tanaka for sharing the FUW-lba1-M2rtTA vector; Dr. K. Inoue for sharing BV2 cells; Y. Nakagawa for excellent secretarial assistance; I. Smith for proofreading the manuscript; Dr. F. D. Costantini for sharing Rosa-YFP reporter mice; Dr. K. Hayashi and Dr. G. Nagamatsu for technical help; L. Cong, S. Yeung, P. Singh, and A. Rymar (Plexxikon) for providing PLX5622; I. Goto (EPS EKISHIN) for providing the PLX5622-formulated diet; and Dr. K. Sawamoto for valuable comments and support of this project. We appreciate technical assistance from the Research Support Center, Research Center for Human Disease Modeling, Kyushu University Graduate School of Medical Sciences.

AUTHOR CONTRIBUTIONS

Conceptualization, T.M. and K.N.; Methodology, T.M. and K.N.; Software, T.M., N.H., and T. Imamura; Validation, T.M. and K.N.; Investigation, T.M., T. Irie, A.M.D.A., S.K., and Y.H.; Formal Analysis, T.M.; Data Curation, T.M.; Writing – Original Draft, T.M. and K.N.; Resources, T.M., H.K., K.S., T.T., H.M., T. Ito, K.I., and K.N.; Visualization, T.M.; Supervision, T.M. and K.N.; Funding Acquisition, T.M. and K.N.

DECLARATION OF INTERESTS

The authors declare no competing interests.

Received: January 30, 2018

Revised: October 23, 2018

Accepted: December 5, 2018

Published: January 9, 2019

REFERENCES

- Agoston, Z., Heine, P., Brill, M.S., Grebbin, B.M., Hau, A.C., Kallenborn-Gerhardt, W., Schramm, J., Götz, M., and Schulte, D. (2014). Meis2 is a Pax6 co-factor in neurogenesis and dopaminergic periglomerular fate specification in the adult olfactory bulb. *Development* 141, 28–38.
- Ambasudhan, R., Talantova, M., Coleman, R., Yuan, X., Zhu, S., Lipton, S.A., and Ding, S. (2011). Direct reprogramming of adult human fibroblasts to functional neurons under defined conditions. *Cell Stem Cell* 9, 113–118.
- Annunziato, L., Boscia, F., and Pignataro, G. (2013). Ionic transporter activity in astrocytes, microglia, and oligodendrocytes during brain ischemia. *J. Cereb. Blood Flow Metab.* 33, 969–982.
- Bailey, T.L., Boden, M., Buske, F.A., Frith, M., Grant, C.E., Clementi, L., Ren, J., Li, W.W., and Noble, W.S. (2009). MEME SUITE: tools for motif discovery and searching. *Nucleic Acids Res.* 37, W202–W208.
- Bakri, Y., Sarrazin, S., Mayer, U.P., Tillmanns, S., Nerlov, C., Boned, A., and Sieweke, M.H. (2005). Balance of MafB and PU.1 specifies alternative macrophage or dendritic cell fate. *Blood* 105, 2707–2716.
- Bennett, M.L., Bennett, F.C., Liddelow, S.A., Ajami, B., Zamaniyan, J.L., Fernhoff, N.B., Mulinyawe, S.B., Bohlen, C.J., Adil, A., Tucker, A., et al. (2016). New tools for studying microglia in the mouse and human CNS. *Proc. Natl. Acad. Sci. USA* 113, E1738–E1746.
- Berninger, B., Costa, M.R., Koch, U., Schroeder, T., Sutor, B., Grothe, B., and Götz, M. (2007). Functional properties of neurons derived from *in vitro* reprogrammed postnatal astroglia. *J. Neurosci.* 27, 8654–8664.
- Bernstein, B.E., Mikkelsen, T.S., Xie, X., Kamal, M., Huebert, D.J., Cuff, J., Fry, B., Meissner, A., Wernig, M., Plath, K., et al. (2006). A bivalent chromatin structure marks key developmental genes in embryonic stem cells. *Cell* 125, 315–326.
- Brulet, R., Matsuda, T., Zhang, L., Miranda, C., Giacca, M., Kaspar, B.K., Nakashima, K., and Hsieh, J. (2017). NEUROD1 instructs neuronal conversion in non-reactive astrocytes. *Stem Cell Reports* 8, 1506–1515.
- Chronis, C., Fiziev, P., Papp, B., Butz, S., Bonora, G., Sabri, S., Ernst, J., and Plath, K. (2017). Cooperative binding of transcription factors orchestrates reprogramming. *Cell* 168, 442–459.e20.
- Cirillo, L.A., Lin, F.R., Cuesta, I., Friedman, D., Jarnik, M., and Zaret, K.S. (2002). Opening of compacted chromatin by early developmental transcription factors HNF3 (FoxA) and GATA-4. *Mol. Cell* 9, 279–289.
- Cregg, J.M., DePaul, M.A., Filous, A.R., Lang, B.T., Tran, A., and Silver, J. (2014). Functional regeneration beyond the glial scar. *Exp. Neurol.* 253, 197–207.
- Eden, E., Navon, R., Steinfeld, I., Lipson, D., and Yakhini, Z. (2009). GOrilla: a tool for discovery and visualization of enriched GO terms in ranked gene lists. *BMC Bioinformatics* 10, 48.
- Foshay, K.M., Looney, T.J., Chari, S., Mao, F.F., Lee, J.H., Zhang, L., Fernandes, C.J., Baker, S.W., Clift, K.L., Gaetz, J., et al. (2012). Embryonic stem cells induce pluripotency in somatic cell fusion through biphasic reprogramming. *Mol. Cell* 46, 159–170.
- Goldberg, A.D., Allis, C.D., and Bernstein, E. (2007). Epigenetics: a landscape takes shape. *Cell* 128, 635–638.
- Guo, Z., Zhang, L., Wu, Z., Chen, Y., Wang, F., and Chen, G. (2014). *In vivo* direct reprogramming of reactive glial cells into functional neurons after brain injury and in an Alzheimer's disease model. *Cell Stem Cell* 14, 188–202.
- Hayashi, Y., Morinaga, S., Zhang, J., Satoh, Y., Meredith, A.L., Nakata, T., Wu, Z., Kohsaka, S., Inoue, K., and Nakanishi, H. (2016). BK channels in microglia are required for morphine-induced hyperalgesia. *Nat. Commun.* 7, 11697.
- Heinrich, C., Blum, R., Gascon, S., Masserdotti, G., Tripathi, P., Sanchez, R., Tiedt, S., Schroeder, T., Götz, M., and Berninger, B. (2010). Directing astroglia from the cerebral cortex into subtype specific functional neurons. *PLoS Biol.* 8, e1000373.
- Hockemeyer, D., Soldner, F., Cook, E.G., Gao, Q., Mitalipova, M., and Jaenisch, R. (2008). A drug-inducible system for direct reprogramming of human somatic cells to pluripotency. *Cell Stem Cell* 3, 346–353.
- Huang, W., Sherman, B.T., and Lempicki, R.A. (2009). Systematic and integrative analysis of large gene lists using DAVID bioinformatics resources. *Nat. Protoc.* 4, 44–57.
- Huang, Y., Xu, Z., Xiong, S., Sun, F., Qin, G., Hu, G., Wang, J., Zhao, L., Liang, Y.X., Wu, T., et al. (2018). Repopulated microglia are solely derived from the proliferation of residual microglia after acute depletion. *Nat. Neurosci.* 21, 530–540.
- Iqbal, A.J., McNeill, E., Kapellos, T.S., Regan-Komito, D., Norman, S., Burd, S., Smart, N., Machemer, D.E., Stylianou, E., McShane, H., et al. (2014). Human CD68 promoter GFP transgenic mice allow analysis of monocyte to macrophage differentiation *in vivo*. *Blood* 124, e33–e44.
- Itoh, Y., Moriyama, Y., Hasegawa, T., Endo, T.A., Toyoda, T., and Gotoh, Y. (2013). Scratch regulates neuronal migration onset via an epithelial-mesenchymal transition-like mechanism. *Nat. Neurosci.* 16, 416–425.
- Kaikkonen, M.U., Spann, N.J., Heinz, S., Romanoski, C.E., Allison, K.A., Stender, J.D., Chun, H.B., Tough, D.F., Prinjha, R.K., Benner, C., and Glass, C.K. (2013). Remodeling of the enhancer landscape during macrophage activation is coupled to enhancer transcription. *Mol. Cell* 51, 310–325.
- Kawano, H., Oyabu, K., Yamamoto, H., Eto, K., Adaniya, Y., Kubota, K., Watanabe, T., Hirano-Iwata, A., Nabekura, J., Katsurabayashi, S., and Iwasaki, K. (2017). Astrocytes with previous chronic exposure to amyloid β -peptide fragment 1–40 suppress excitatory synaptic transmission. *J. Neurochem.* 143, 624–634.
- Kim, D., Pertea, G., Trapnell, C., Pimentel, H., Kelley, R., and Salzberg, S.L. (2013). TopHat2: accurate alignment of transcriptomes in the presence of insertions, deletions and gene fusions. *Genome Biol.* 14, R36.
- Kimura, H., Hayashi-Takanaka, Y., Goto, Y., Takizawa, N., and Nozaki, N. (2008). The organization of histone H3 modifications as revealed by a panel of specific monoclonal antibodies. *Cell Struct. Funct.* 33, 61–73.
- Koche, R.P., Smith, Z.D., Adli, M., Gu, H., Ku, M., Gnrke, A., Bernstein, B.E., and Meissner, A. (2011). Reprogramming factor expression initiates widespread targeted chromatin remodeling. *Cell Stem Cell* 8, 96–105.
- Langlais, D., Barreiro, L.B., and Gros, P. (2016). The macrophage IRF8/IRF1 regulome is required for protection against infections and is associated with chronic inflammation. *J. Exp. Med.* 213, 585–603.
- Langmead, B., and Salzberg, S.L. (2012). Fast gapped-read alignment with Bowtie 2. *Nat. Methods* 9, 357–359.
- Lavin, Y., Winter, D., Blecher-Gonen, R., David, E., Keren-Shaul, H., Merad, M., Jung, S., and Amit, I. (2014). Tissue-resident macrophage enhancer landscapes are shaped by the local microenvironment. *Cell* 159, 1312–1326.
- Li, H., Handsaker, B., Wysoker, A., Fennell, T., Ruan, J., Homer, N., Marth, G., Abecasis, G., and Durbin, R.; 1000 Genome Project Data Processing Subgroup (2009). The Sequence Alignment/Map format and SAMtools. *Bioinformatics* 25, 2078–2079.
- Liu, M.L., Zang, T., Zou, Y., Chang, J.C., Gibson, J.R., Huber, K.M., and Zhang, C.L. (2013). Small molecules enable neurogenin 2 to efficiently convert human fibroblasts into cholinergic neurons. *Nat. Commun.* 4, 2183.
- Ma, H., Morey, R., O'Neill, R.C., He, Y., Daughtry, B., Schultz, M.D., Hariharan, M., Nery, J.R., Castanon, R., Sabatini, K., et al. (2014). Abnormalities in human pluripotent cells due to reprogramming mechanisms. *Nature* 511, 177–183.
- Mall, M., Karefa, M.S., Chanda, S., Ahlenius, H., Perotti, N., Zhou, B., Grieder, S.D., Ge, X., Drake, S., Euong Ang, C., et al. (2017). Myt1l safeguards neuronal identity by actively repressing many non-neuronal fates. *Nature* 544, 245–249.
- Mancino, A., Termanini, A., Barozzi, I., Ghisletti, S., Ostuni, R., Prosperini, E., Ozato, K., and Natoli, G. (2015). A dual *cis*-regulatory code links IRF8 to constitutive and inducible gene expression in macrophages. *Genes Dev.* 29, 394–408.
- Masuda, T., Tsuda, M., Yoshinaga, R., Tozaki-Saitoh, H., Ozato, K., Tamura, T., and Inoue, K. (2012). IRF8 is a critical transcription factor for transforming microglia into a reactive phenotype. *Cell Rep.* 1, 334–340.
- Matcovitch-Natan, O., Winter, D.R., Giladi, A., Vargas Aguilar, S., Spinrad, A., Sarrazin, S., Ben-Yehuda, H., David, E., Zelada González, F., Perrin, P., et al.

- (2016). Microglia development follows a stepwise program to regulate brain homeostasis. *Science* 353, aad8670.
- Matsuda, T., Murao, N., Katano, Y., Juliandi, B., Kohyama, J., Akira, S., Kawai, T., and Nakashima, K. (2015). TLR9 signalling in microglia attenuates seizure-induced aberrant neurogenesis in the adult hippocampus. *Nat. Commun.* 6, 6514.
- McLean, C.Y., Bristor, D., Hiller, M., Clarke, S.L., Schaar, B.T., Lowe, C.B., Wenger, A.M., and Bejerano, G. (2010). GREAT improves functional interpretation of cis-regulatory regions. *Nat. Biotechnol.* 28, 495–501.
- Menéndez-Gutiérrez, M.P., Rószer, T., Fuentes, L., Núñez, V., Escolano, A., Redondo, J.M., De Clerck, N., Metzger, D., Valledor, A.F., and Ricote, M. (2015). Retinoid X receptors orchestrate osteoclast differentiation and postnatal bone remodeling. *J. Clin. Invest.* 125, 809–823.
- Mikkelsen, T.S., Ku, M., Jaffe, D.B., Issac, B., Lieberman, E., Giannoukos, G., Alvarez, P., Brockman, W., Kim, T.K., Koche, R.P., et al. (2007). Genome-wide maps of chromatin state in pluripotent and lineage-committed cells. *Nature* 448, 553–560.
- Miura, F., Enomoto, Y., Dairiki, R., and Ito, T. (2012). Amplification-free whole-genome bisulfite sequencing by post-bisulfite adaptor tagging. *Nucleic Acids Res.* 40, e136.
- Mohn, F., Weber, M., Rebhan, M., Roloff, T.C., Richter, J., Stadler, M.B., Bibel, M., and Schübeler, D. (2008). Lineage-specific polycomb targets and de novo DNA methylation define restriction and potential of neuronal progenitors. *Mol. Cell* 30, 755–766.
- Ng, S.L., Friedman, B.A., Schmid, S., Gertz, J., Myers, R.M., Tenover, B.R., and Maniatis, T. (2011). IκB kinase epsilon (IKK(epsilon)) regulates the balance between type I and type II interferon responses. *Proc. Natl. Acad. Sci. USA* 108, 21170–21175.
- Niu, W., Zang, T., Zou, Y., Fang, S., Smith, D.K., Bachoo, R., and Zhang, C.L. (2013). In vivo reprogramming of astrocytes to neuroblasts in the adult brain. *Nat. Cell Biol.* 15, 1164–1175.
- Niu, W., Zang, T., Smith, D.K., Vue, T.Y., Zou, Y., Bachoo, R., Johnson, J.E., and Zhang, C.L. (2015). SOX2 reprograms resident astrocytes into neural progenitors in the adult brain. *Stem Cell Reports* 4, 780–794.
- Oki, S., Ohta, T., Shioi, G., Hatanaka, H., Ogasawara, O., Okuda, Y., Kawaji, H., Nakaki, R., Sese, J., and Meno, C. (2018). ChIP-Atlas: a data-mining suite powered by full integration of public ChIP-seq data. *EMBO Rep.* 19, 46255.
- Ostuni, R., Piccolo, V., Barozzi, I., Polletti, S., Termanini, A., Bonifacio, S., Curina, A., Prosperini, E., Ghisletti, S., and Natoli, G. (2013). Latent enhancers activated by stimulation in differentiated cells. *Cell* 152, 157–171.
- Pang, Z.P., Yang, N., Vierbuchen, T., Ostermeier, A., Fuentes, D.R., Yang, T.Q., Citri, A., Sebastian, V., Marro, S., Südhof, T.C., and Wernig, M. (2011). Induction of human neuronal cells by defined transcription factors. *Nature* 476, 220–223.
- Papp, B., and Müller, J. (2006). Histone trimethylation and the maintenance of transcriptional ON and OFF states by trxG and Pcg proteins. *Genes Dev.* 20, 2041–2054.
- Patel, R.K., and Jain, M. (2012). NGS QC Toolkit: a toolkit for quality control of next generation sequencing data. *PLoS ONE* 7, e30619.
- Qin, X.F., An, D.S., Chen, I.S., and Baltimore, D. (2003). Inhibiting HIV-1 infection in human T cells by lentiviral-mediated delivery of small interfering RNA against CCR5. *Proc. Natl. Acad. Sci. USA* 100, 183–188.
- Rais, Y., Zvir'an, A., Geula, S., Gafni, O., Chomsky, E., Viukov, S., Mansour, A.A., Caspi, I., Krupalnik, V., Zerbib, M., et al. (2013). Deterministic direct reprogramming of somatic cells to pluripotency. *Nature* 502, 65–70.
- Robel, S., Berninger, B., and Götz, M. (2011). The stem cell potential of glia: lessons from reactive gliosis. *Nat. Rev. Neurosci.* 12, 88–104.
- Sanosaka, T., Immamura, T., Hamazaki, N., Chai, M., Igarashi, K., Ideta-Otsuka, M., Miura, F., Ito, T., Fujii, N., Ikeo, K., and Nakashima, K. (2017). DNA methylome analysis identifies transcription factor-based epigenomic signatures of multilineage competence in neural stem/progenitor cells. *Cell Rep.* 20, 2992–3003.
- Schmitges, F.W., Prusty, A.B., Faty, M., Stützer, A., Lingaraju, G.M., Aiwasian, J., Sack, R., Hess, D., Li, L., Zhou, S., et al. (2011). Histone methylation by PRC2 is inhibited by active chromatin marks. *Mol. Cell* 42, 330–341.
- Schütte, J., Wang, H., Antoniou, S., Jarratt, A., Wilson, N.K., Riepsaame, J., Calero-Nieto, F.J., Moignard, V., Basilico, S., Kinston, S.J., et al. (2016). An experimentally validated network of nine haematopoietic transcription factors reveals mechanisms of cell state stability. *eLife* 5, e11469.
- Shen, L., Shao, N., Liu, X., and Nestler, E. (2014). ngs.plot: Quick mining and visualization of next-generation sequencing data by integrating genomic databases. *BMC Genomics* 15, 284.
- Simonsson, S., and Gurdon, J. (2004). DNA demethylation is necessary for the epigenetic reprogramming of somatic cell nuclei. *Nat. Cell Biol.* 6, 984–990.
- Smith, D.K., Yang, J., Liu, M.L., and Zhang, C.L. (2016). Small molecules modulate chromatin accessibility to promote NEUROG2-mediated fibroblast-to-neuron reprogramming. *Stem Cell Reports* 7, 955–969.
- Sofroniew, M.V. (2009). Molecular dissection of reactive astrogliosis and glial scar formation. *Trends Neurosci.* 32, 638–647.
- Soucie, E.L., Weng, Z., Geirsdóttir, L., Molawi, K., Maurizio, J., Fenouil, R., Mossadeq-Keller, N., Gimenez, G., VanHille, L., Beniazza, M., et al. (2016). Lineage-specific enhancers activate self-renewal genes in macrophages and embryonic stem cells. *Science* 351, aad5510.
- Srinivasan, S., Dorighi, K.M., and Tamkun, J.W. (2008). *Drosophila* Kismet regulates histone H3 lysine 27 methylation and early elongation by RNA polymerase II. *PLoS Genet.* 4, e1000217.
- Stadtfeld, M., Maherli, N., Breault, D.T., and Hochedlinger, K. (2008). Defining molecular cornerstones during fibroblast to iPS cell reprogramming in mouse. *Cell Stem Cell* 2, 230–240.
- Su, Z., Niu, W., Liu, M.L., Zou, Y., and Zhang, C.L. (2014). In vivo conversion of astrocytes to neurons in the injured adult spinal cord. *Nat. Commun.* 5, 3338.
- Takahashi, K., and Yamanaka, S. (2006). Induction of pluripotent stem cells from mouse embryonic and adult fibroblast cultures by defined factors. *Cell* 126, 663–676.
- Tanaka, K.F., Matsui, K., Sasaki, T., Sano, H., Sugio, S., Fan, K., Hen, R., Nakai, J., Yanagawa, Y., Hasuwa, H., et al. (2012). Expanding the repertoire of optogenetically targeted cells with an enhanced gene expression system. *Cell Rep.* 2, 397–406.
- Trapnell, C., Hendrickson, D.G., Sauvageau, M., Goff, L., Rinn, J.L., and Pachter, L. (2013). Differential analysis of gene regulation at transcript resolution with RNA-seq. *Nat. Biotechnol.* 31, 46–53.
- Vierbuchen, T., Ostermeier, A., Pang, Z.P., Kokubu, Y., Südhof, T.C., and Wernig, M. (2010). Direct conversion of fibroblasts to functional neurons by defined factors. *Nature* 463, 1035–1041.
- Voigt, P., Tee, W.W., and Reinberg, D. (2013). A double take on bivalent promoters. *Genes Dev.* 27, 1318–1338.
- Wang, L.L., Su, Z., Tai, W., Zou, Y., Xu, X.M., and Zhang, C.L. (2016). The p53 pathway controls SOX2-mediated reprogramming in the adult mouse spinal cord. *Cell Rep.* 17, 891–903.
- Wapinski, O.L., Vierbuchen, T., Qu, K., Lee, Q.Y., Chanda, S., Fuentes, D.R., Giresi, P.G., Ng, Y.H., Marro, S., Neff, N.F., et al. (2013). Hierarchical mechanisms for direct reprogramming of fibroblasts to neurons. *Cell* 155, 621–635.
- White, R.E., Rao, M., Gensel, J.C., McTigue, D.M., Kaspar, B.K., and Jakeman, L.B. (2011). Transforming growth factor α transforms astrocytes to a growth-supportive phenotype after spinal cord injury. *J. Neurosci.* 31, 15173–15187.
- Yin, Y., Morgunova, E., Jolma, A., Kaasinen, E., Sahu, B., Khund-Sayeed, S., Das, P.K., Kivioja, T., Dave, K., Zhong, F., et al. (2017). Impact of cytosine methylation on DNA binding specificities of human transcription factors. *Science* 356, eaaj2239.
- Zaret, K.S., and Carroll, J.S. (2011). Pioneer transcription factors: establishing competence for gene expression. *Genes Dev.* 25, 2227–2241.

- Zhang, Y., Liu, T., Meyer, C.A., Eeckhoute, J., Johnson, D.S., Bernstein, B.E., Nusbaum, C., Myers, R.M., Brown, M., Li, W., and Liu, X.S. (2008). Model-based analysis of ChIP-Seq (MACS). *Genome Biol.* 9, R137.
- Zhang, Y., Chen, K., Sloan, S.A., Bennett, M.L., Scholze, A.R., O'Keeffe, S., Phatnani, H.P., Guarnieri, P., Caneda, C., Ruderisch, N., et al. (2014). An RNA-sequencing transcriptome and splicing database of glia, neurons, and vascular cells of the cerebral cortex. *J. Neurosci.* 34, 11929–11947.
- Zhang, M., Lin, Y.H., Sun, Y.J., Zhu, S., Zheng, J., Liu, K., Cao, N., Li, K., Huang, Y., and Ding, S. (2016). Pharmacological reprogramming of fibroblasts into neural stem cells by signaling-directed transcriptional activation. *Cell Stem Cell* 18, 653–667.
- Zohren, F., Souroullas, G.P., Luo, M., Gerdemann, U., Imperato, M.R., Wilson, N.K., Göttgens, B., Lukov, G.L., and Goodell, M.A. (2012). The transcription factor Lyl-1 regulates lymphoid specification and the maintenance of early T lineage progenitors. *Nat. Immunol.* 13, 761–769.

STAR★METHODS

KEY RESOURCES TABLE

REAGENT or RESOURCE	SOURCE	IDENTIFIER
Antibodies		
Goat polyclonal anti-Iba1	Abcam	Cat# ab5076; RRID: AB_2224402
Chick polyclonal anti-GFAP	Merck Millipore	Cat# AB5541; RRID: AB_177521
Rabbit polyclonal anti-βIII-tubulin	Covance	Cat# PRB-435P; RRID: AB_291637
Rat monoclonal anti-CD11b	Bio-Rad	Cat# MCA711G; RRID: AB_323167
Goat polyclonal anti-Olig2	R&D Systems	Cat# AF2418; RRID: AB_2157554
Rat monoclonal anti-CD68	Bio-Rad	Cat# MCA1957; RRID: AB_322219
Mouse monoclonal anti-Nestin	Merck Millipore	Cat# MAB5326; RRID: AB_11211837
Rabbit polyclonal Anti-Map2	Merck Millipore	Cat# AB5622; RRID: 91939
Guinea pig polyclonal anti-DCX	Merck Millipore	Cat# AB2253; RRID: AB_1586992
Mouse monoclonal anti-MAP2ab	Sigma	Cat# M1406; RRID: AB_477171
Chick polyclonal anti-GFP	Aves	Cat# GFP-1020; RRID: AB_10000240
Mouse monoclonal anti-GAD67	Merck Millipore	Cat# MAB5406; RRID: AB_2278725
Guinea pig polyclonal anti-VGLUT1	Merck Millipore	Cat# AB5905; RRID: AB_2301751
Mouse monoclonal anti-NeuN	Merck Millipore	Cat# MAB377; RRID: AB_2298772
Rabbit monoclonal anti-PSD95	Cell Signaling Technology	Cat#3409; RRID: AB_1264242
Mouse monoclonal anti-H3K4me3	MBL	Cat#MABI0304; RRID: AB_11123891
Mouse monoclonal anti-H3K27me3	MBL	Cat#MABI0323; RRID: AB_11123929
Mouse monoclonal anti-H3K27ac	MBL	Cat#MABI0309; RRID: AB_11126964
Mouse monoclonal anti-H3K4me1	MBL	Cat#MABI0302; RRID: AB_11126551
Mouse monoclonal anti-FLAG	Sigma	Cat#F1804; RRID: AB_262044
Rabbit monoclonal anti-Tmem119	Abcam	Cat#ab209064; RRID: AB_2728083
Rabbit monoclonal anti-DARPP32	Abcam	Cat#ab40801; RRID: AB_731843
Mouse monoclonal anti-PSD95	Abcam	Cat#ab2723; RRID: AB_303248
Mouse monoclonal anti-APC	CALBIOCHEM	Cat#OP80; RRID: AB_2057371
Mouse monoclonal anti-MBP	Millipore	Cat#AB980; RRID: AB_92396
Rabbit polyclonal anti-active Caspase3	R&D Systems	Cat#AF835; RRID: AB_2243952
Bacterial and Virus Strains		
<i>E. coli</i> Stbl3	Thermo Fisher	Cat# C737303
<i>E. coli</i> DH5α	Toyobo	Cat# DNA-913
Chemicals, Peptides, and Recombinant Proteins		
BDNF	Peprotech	450-02
GDNF	Peprotech	450-10
NT3	Peprotech	450-03
bFGF	Peprotech	100-18
EGF	Peprotech	AF-100-15
PDGF-AA	Peprotech	100-13
Deposited Data		
RNA-seq data	This study	GSE104435
WGBS data	This study	GSE104435
ChIP-seq data	This study	GSE104435
Experimental Models: Cell Lines		
BV2 (microglial cell line)	Gift from Dr. Inoue (Masuda et al., 2012)	N/A
HEK293T	ATCC	Cat# CRL-3216

(Continued on next page)

Continued

REAGENT or RESOURCE	SOURCE	IDENTIFIER
Experimental Models: Organisms/Strains		
Mouse: C57BL/6	Japan SLC	N/A
Mouse: ICR	Japan SLC	N/A
Oligonucleotides		
Primers for RT-PCR, see Table S4	This study	N/A
Lyl1 sh1 GAGGAAACGCCCTGTAGCTCT	This study	N/A
Lyl1 sh2 GCGCTTGATCCATGATCCTGT	This study	N/A
Mafb sh1 CGGCCTTGACCTGTTGA CTTGA	This study	N/A
Mafb sh2 GCAAGCTGAGTCTTGTGG	This study	N/A
Batf3 sh1 GAGTCGTTCTCTCTCACTT	This study	N/A
Batf3 sh2 GGACGATGACAGGAAAGTCG	This study	N/A
Brn2 sh1 CTCGGATTACTCAAGCAG	This study	N/A
Brn2 sh2 CTTCAAGAACATGTGCAAGC	This study	N/A
Recombinant DNA		
Tet-O-FUW ND1	Vierbuchen et al., 2010	Addgene #30129
Tet-O-FUW Ascl1	Vierbuchen et al., 2010	Addgene #27150
Tet-O-FUW Brn2	Vierbuchen et al., 2010	Addgene #27151
Tet-O-FUW Myt1l	Vierbuchen et al., 2010	Addgene #27152
Tet-O-FUW Olig2	Vierbuchen et al., 2010	Addgene #30131
Tet-O-FUW Zic1	Vierbuchen et al., 2010	Addgene #30132
Tet-O-FUW EGFP	Vierbuchen et al., 2010	Addgene #30130
FUW-M2rtTA	Hockemeyer et al., 2008	Addgene #20342
Tet-O-FUW Neurog2	This study	N/A
Tet-O-FUW Sox2	This study	N/A
Tet-O-FUW Blh22	This study	N/A
Tet-O-FUW Prdm8	This study	N/A
Tet-O-FUW Mycn	This study	N/A
Tet-O-FUW FLAG-Scr1	This study	N/A
Tet-O-FUW FLAG-Meis2	This study	N/A
Tet-O-FUW Scr1	This study	N/A
Tet-O-FUW Meis2	This study	N/A
Tet-O-FUW tdTomato	This study	N/A
Tet-O-FUW FLAG-ND1	This study	N/A
pLLX lyl1 sh1	This study	N/A
pLLX lyl1 sh2	This study	N/A
pLLX Mafb sh1	This study	N/A
pLLX Mafb sh2	This study	N/A
pLLX Batf3 sh1	This study	N/A
pLLX Batf3 sh2	This study	N/A
pLLX Brn2 sh1	This study	N/A
pLLX Brn2 sh2	This study	N/A
FUW- <i>Iba1</i> -M2rtTA	Gift from Dr. Tanaka (Tanaka et al., 2012)	N/A
FG12 human CD68-ND1-P2A-EGFP	This study	N/A
FG12 human CD68-EGFP	This study	N/A
FG12 human CD68-ND1	This study	N/A
FG12	Qin et al., 2003	Addgene #14884

(Continued on next page)

Continued

REAGENT or RESOURCE	SOURCE	IDENTIFIER
Software and Algorithms		
GREAT	McLean et al., 2010	http://bejerano.stanford.edu/great/public/html/
Bowtie v2	Langmead and Salzberg, 2012	http://bowtie-bio.sourceforge.net/bowtie2/index.shtml
TopHat2	Kim et al., 2013	https://ccb.jhu.edu/software/tophat/index.shtml
MACS14 1.4.2	Zhang et al., 2008	https://github.com/taoliu/MACS
MEME	Bailey et al., 2009	http://meme-suite.org/index.html
SAMtools	Li et al., 2009	http://samtools.sourceforge.net/
Cufflinks v2.1.1	Trapnell et al., 2013	http://cole-trapnell-lab.github.io/cufflinks/
BMap	Miura et al., 2012	http://itolab.med.kyushu-u.ac.jp/BMap/get.html
DAVID	Huang et al., 2009	https://david.ncifcrf.gov/
GORilla	Eden et al., 2009	http://cbl-gorilla.cs.technion.ac.il/
ChIP-Atlas	Oki et al., 2018	http://chip-atlas.org/

CONTACT FOR REAGENT AND RESOURCE SHARING

Further information and requests for resources should be directed to and will be fulfilled by the Lead Contact, Kinichi Nakashima (kin1@scb.med.kyushu-u.ac.jp).

EXPERIMENTAL MODEL AND SUBJECT DETAILS**Mice**

All efforts were made to minimize animal suffering and to reduce the number of animals used. Animals were housed under a 12/12-h light/dark cycle and fed *ad libitum*. For *in vitro* studies, we used sex-unspecified wild-type mice at postnatal day 1 (C57/BL6 or ICR obtained from Japan SLC). Male 8-week-old wild-type mice (C57BL/6 obtained from Japan SLC) and Rosa-YFP reporter mice (a generous gift from Dr. F. D. Costantini) were used for *in vivo* lentiviral injections. All experiments were carried out according to the animal experimentation guidelines of Kyushu University, which comply with the National Institutes of Health Guide for the Care and Use of Laboratory Animals.

Primary Cells

We prepared primary microglia, neurons, astrocytes and oligodendrocytes from mouse at postnatal day 1 (P1). Astrocytes and microglia were cultured with DMEM (Nacalai Tesque) containing 10% FBS. Neurons were cultured with maintenance medium (Neurobasal Medium (GIBCO) supplemented with B27 (GIBCO)). Oligodendrocyte precursor cells (OPCs) were cultured with DMEM/F12 (Nacalai Tesque) supplemented with insulin (25 µg/ml, Sigma), apo-transferrin (100 µg/ml, Sigma), progesterone (20 nM, Sigma), putrescine (60 µM, Sigma), sodium selenite (30 nM, Sigma), human PDGF-AA (10 ng/ml, Peprotech), bFGF (20 ng/ml, Peprotech) and EGF (20 ng/ml, Peprotech). For oligodendrocyte differentiation, triiodo-L-thyronine (T3; 50 ng/ml, Sigma) and L-thyroxine (T4; 50 ng/ml, Sigma) were added to the medium and cultured for 7 days.

Cell Lines

HEK293T human embryonic kidney cells (available source material information: fetus) were obtained from American Type Culture Collection (ATCC) cat# CRL-3216. HEK293T cells were grown in DMEM (Nacalai Tesque) supplemented with 10% FBS. Microglial cell line BV2 (available source material information: C57BL/6 female mouse) was gifted from Dr. K. Inoue and cultured with DMEM containing 5% FBS.

METHOD DETAILS**Primary cell isolation and culture**

We prepared primary microglia, neurons, astrocytes and oligodendrocytes from mouse at postnatal day 1 (P1) using a previously published protocol ([Matsuda et al., 2015](#)), with some modifications. To obtain mixed glial cell cultures, cortices of C57/BL6 or

ICR mice were carefully dissected after stripping of meninges. The tissue was digested with papain (Sigma) at 37°C for 20 min. After centrifugation (200g, 5 min), the cell pellet was suspended in alpha-minimum essential medium (MEM) with 5% fetal bovine serum (FBS) and 0.6% glucose, and the suspension was passed through a 40-μm Cell Strainer (BD Falcon). After centrifugation (200 g, 5 min), the cell pellet was resuspended in DMEM containing 10% FBS and a low concentration of GM-SCF (0.1 ng/ml; PeproTech) to enhance microglial proliferation. These mixed glial cells were plated in T75 tissue culture flasks. The medium was renewed every 2–3 days. Seven days after plating, microglia and OPCs were detached from astrocyte monolayer sheets by shaking for 1 h and then collected and plated onto uncoated 35-mm culture dishes to remove OPCs. After a 30-min incubation, the medium was removed by suction and DMEM containing 10% FBS (microglial medium) was added to the dish. These primary cultured microglia were used for neuronal conversion. After the shake-off procedure for the isolation of microglia, the cells were treated with AraC (5 μM) to eliminate proliferating cells for a total of 2 days. Cultures were shaken once more, and then Trypsin EDTA solution was added to the flask to obtain the remaining astrocytes, which were transferred to a 35-mm culture dish and maintained in DMEM containing 10% FBS. Two days after plating, the astrocytes were used for assays. To obtain oligodendrocytes, OPCs were plated in a poly-L-lysine-coated 35-mm culture dish and cultured with DMEM/F12 supplemented with insulin (25 μg/ml), apo-transferrin (100 μg/ml), progesterone (20 nM), putrescine (60 μM), sodium selenite (30 nM), human PDGF-AA (10 ng/ml, Peprotech), bFGF (20 ng/ml, Peprotech) and EGF (20 ng/ml, Peprotech). For oligodendrocyte differentiation, triiodo-L-thyronine (T3; 50 ng/ml, Sigma-Aldrich) and L-thyroxine (T4; 50 ng/ml, Sigma-Aldrich) were added to the medium and cultured for 7 days.

Neuronal cultures were prepared from P1 mouse cortex according to a previously described protocol, with some modification (Matsuda et al., 2015). The cortices were digested with papain at 37°C for 20 min and triturated with a 1 mL pipette. MEM with 5% FBS and 0.6% glucose was added and the mixture was plated onto a poly-L-lysine-coated 35-mm culture dish. After 3 h, the medium was replaced with maintenance medium (Neurobasal Medium (GIBCO) supplemented with B27 (GIBCO)) containing cytosine b-D-arabinofuranoside (5 mM; Sigma) to eliminate proliferating cells. To avoid neuronal cell death by a complete medium change, half of the medium was replaced every 3 days with fresh maintenance medium.

iN cell induction

To induce iN cells, we used lentiviral vectors that control gene expression under the tetracycline operator. Plasmids for the candidate factors Ascl1, ND1, Brn2, Myt1l, Olig2 and Zic1 were obtained from Addgene. cDNAs for other candidate factors were cloned into the Tet-O-FUW vector using EcoRI sites. Lentivirus vectors used to express short hairpin (sh)RNA for MBD3, miR-124, Lyl1 (Lyl1 sh1 and sh2), Mafb (Mafb sh1 and sh2) and Batf3 (Batf3 sh1 and sh2) were cloned into the pLLX vector, a generous gift from M. E. Greenberg. Lentiviruses were produced by transfecting HEK293T cells with the lentivirus constructs pCMV-VSV-G-RSV-Rev and pCAG-HIVgp using polyethylenimine. Primary cultured microglia were infected with candidate factor-expressing lentivirus constructs together with an M2rtTA-expressing lentivirus construct (Addgene) in microglia medium containing polybrene (8 μg/ml). After 16–20 h in medium containing lentivirus, the medium was replaced with iN medium, which consists of Neurobasal Medium (GIBCO), B27 (GIBCO), BDNF, GDNF, NT3 (10 ng/ml each, Peprotech) and penicillin/streptomycin/fungizone (HyClone). Doxycycline (2 mg/ml) was added only once to this medium to activate expression of the transduced genes. The medium was changed every 2–3 days for the duration of the culture period. To induce specific ND1 expression in microglia, we used lentivirus carrying M2rtTA under the control of the *Iba1* promoter, which was provided by K.F. Tanaka (Tanaka et al., 2012). To induce activation of microglia, LPS (Sigma) was added to the medium for 12 h before lentiviral infections.

Knockdown experiments

To knock down Lyl1, Mafb and Batf3 expression, shRNA for Lyl1 (Lyl1 sh1 and sh2), Mafb (Mafb sh1 and sh2), Batf3 (Batf3 sh1 and sh2) and Brn2 (Brn2 sh1 and sh2) were cloned into pLLX, which had been modified to express EGFP together with a puromycin resistance gene under the ubiquitin-C promoter. Microglia were infected with shRNA-containing lentivirus and treated one day later with puromycin (2 μg/ml; Sigma, P8833) for an additional 3 days.

Immunocytochemistry

Cells were fixed in 4% paraformaldehyde and processed for immunostaining. Cells were blocked for 1 h at room temperature (RT) with blocking solution (5% FBS and 0.3% Triton X-100), and incubated for 2 h at RT with one of the following primary antibodies: anti-Iba1 (1:500), anti-GFAP (1:500), anti-βIII-tubulin (1:500), anti-CD11b (1:500), anti-Olig2 (1:500), anti-CD68 (1:500), anti-Nestin (1:500), anti-Map2 (1:500), anti-DCX (1:500), anti-Map2ab (1:500), anti-GFP (1:500), anti-GAD67 (1:500), anti-VGLUT1 (1:500), anti-NeuN (1:500) and anti-PSD95 (1:100). Stained cells were visualized with a fluorescence microscope (Zeiss Axiovert 200M, Zeiss).

EdU labeling and detection

For EdU experiments, 10 mM EdU was added to the culture medium and was maintained throughout medium changes until the cells were fixed. EdU staining was performed using a Click-iT EdU Alexa Fluor 555 Imaging Kit (Life Technologies) according to the supplier's protocol. Stained cells were visualized with a fluorescence microscope (Zeiss Axiovert 200M, Zeiss).

Real-time PCR analysis

Total RNA was isolated from cells using Sepasol-RNA I Super G (Nacalai Tesque) following the manufacturer's instructions. RNA quality of all samples was checked by spectrophotometer. Reverse transcription reactions were carried out using a SuperScript VILO cDNA Synthesis Kit (Life Technologies) according to the kit protocol. qRT-PCR was performed with SYBR green fluorescent dye using Step One Plus (Applied Biosystems) and Mx3000 (Stratagene). GAPDH was used as an endogenous control to normalize samples. PCR primers used in this study are listed in [Table S4](#).

Co-culture with primary cultured cortical neurons and calcium imaging

At 16–20 h after lentiviral infection, ND1-transduced microglia were passaged and seeded on primary cultured cortical neurons. Before seeding the microglia, they were washed three times with microglial medium to remove virus particles. To visualize infected microglia, tdTomato cloned into Tet-O-FUW vector was used. Immunocytochemistry and calcium imaging were performed at 3 weeks after Dox treatment. For calcium imaging, cells were washed with recording medium (10 mM HEPES, 140 mM NaCl, 5.0 mM KCl, 1.2 mM MgCl₂, 2 mM CaCl₂, 10 mM glucose) and then incubated with recording medium containing 2 μM Fluo4-AM (Invitrogen) and 0.01% Cremophor-EL (Sigma) for 20 min at RT. The medium was then replaced with fresh recording medium and 100 μM NMDA was added to stimulate cultured neurons. Calcium signals were recorded with a confocal microscope (LSM800, Zeiss).

RNA sequencing and data analysis

Control microglia and ND1-transduced microglia were cultured under iN cell medium. In this study, we employed M2rtTA-transduced microglia as a control. Purified mRNAs were subjected to library construction using the NEBNext Ultra Directional RNA Library Prep Kit for Illumina (New England Biolabs) following the manufacturer's protocols. cDNA libraries were purified using AMPure XP beads (Beckman Coulter). cDNA library quality was assessed using an Agilent 2100 BioAnalyzer (Agilent Technologies). RNA sequencing was performed with 50-bp single-end sequencing by an Illumina HiSeq 2500. Obtained reads were processed with the FASTX tool kit ([Patel and Jain, 2012](#)) to remove short (< 30 bp) and low-quality (quality score < 20) reads, followed by trimming of the adaptor sequence. Processed reads were aligned to mm10 using TopHat ([Kim et al., 2013](#)). Cuffdiff ([Trapnell et al., 2013](#)), a program in Cufflinks, was used for differential gene expression analysis. Pearson's correlation was calculated with R, based on gene expression levels. Gene ontology (GO) analysis was performed using Database for Annotation, Visualization and Integrated Discovery (DAVID) ([Huang et al., 2009](#)). For investigating enriched GO terms in unchanged genes compared to upregulated genes, GOrilla was used ([Eden et al., 2009](#)). We analyzed GO term enrichment in the Biological Process category. To identify microglia- and neuron-specific genes, we used FPKM values of microglia (microglia day 2), neurons, NS/PCs, oligodendrocytes and astrocytes, and calculated genes with at least 2-fold higher FPKM in microglia or neurons than in any other cell types. For analyzing NS/PCs, oligodendrocytes and astrocytes, public RNA-seq data were used in this study ([Zhang et al., 2016](#); [Zhang et al., 2014](#)). To identify ND1 target genes, genes whose expression was less than 1 FPKM in ND1-transduced cells were excluded.

Chromatin immunoprecipitation assay

Cells grown on 10-cm dishes were fixed with 1% formaldehyde-containing medium for 10 min at RT and were then quenched by 125 mM glycine for 5 min at RT. The cells were washed with ice-cold PBS twice, and cold PBS containing protease inhibitor was added. These cells were harvested using a cell scraper and centrifuged at 8000g, 4°C for 10 min. The cell pellet was suspended in 1 mL of buffer 1 (140 mM NaCl, 1 mM EDTA, 50 mM HEPES-KOH (pH 7.5), 0.5% NP-40, 10% glycerol, 0.25% Triton X-100, protease inhibitor) and kept at 4°C for 10 min. After centrifugation as above, the supernatant was discarded and the pellet was suspended in 1 mL of buffer 2 (20 mM Tris-HCl (pH 7.5), 200 mM NaCl, 1 mM EDTA, 0.5 mM EGTA, protease inhibitor). After a third centrifugation, the supernatant was again discarded and the pellet suspended in 400 μL of buffer 3 (20 mM Tris-HCl (pH 7.5), 150 mM NaCl, 1 mM EDTA, 0.5 mM EGTA, 1% Triton X-100, 0.1% Na-deoxycholate, 0.1% SDS, protease inhibitor). After incubation at 4°C for 10 min, the lysates were sonicated with a sonicator (Branson) and then centrifuged at 20,000g, 4°C for 10 min. The supernatant was collected, and 10% of its volume was used for input.

For each ChIP reaction, 50 μL of Dynabeads M-280 sheep anti-mouse IgG (Life Technologies) were washed twice with PBS. Beads were collected magnetically and conjugated to 2 μg of primary antibody in 1.2 mL of PBS with protease inhibitor. The suspensions were rotated at 4°C overnight, after which the beads were collected by magnet and washed twice with 1 mL of ice-cold PBS, once with 1 mL of buffer 3, and then suspended in 600 μL of buffer 3. Sheared chromatin was added to the beads and allowed to react overnight at 4°C with rotation. The immunoprecipitated samples were washed once with buffer 3, twice with buffer 4 (20 mM Tris-HCl (pH 7.5), 500 mM NaCl, 1 mM EDTA, 0.5 mM EGTA, 1% Triton X-100, 0.1% Na-deoxycholate, 0.1% SDS), three times with RIPA buffer (1 mM EDTA, 50 mM HEPES-KOH (pH 7.4), 1% NP-40, 0.25 M LiCl, 0.5% Na-deoxycholate) and once with TE50 buffer (50 mM Tris-HCl (pH 8.0), 10 mM EDTA). Immunoprecipitated DNAs or input DNAs were eluted by adding 100 μL of elution buffer (TE50 buffer, 1% SDS) and incubated at 65°C overnight. Samples were supplemented with 100 μL of TE buffer (10 mM Tris-HCl (pH 8.0), 1 mM EDTA), and treated with RNAase A at 37°C for 1 h and proteinase K at 50°C for 2 h. DNA was purified using a PCR purification kit (QIAGEN) according to the supplier's protocol. The antibodies used for ChIP-qPCR and ChIP-seq were mouse anti-FLAG, mouse anti-H3K27ac, mouse anti-H3K4me1, mouse anti-H3K4me3 and mouse anti-H3K27me3 ([Kimura et al., 2008](#)). PCR primers used in this study are listed in [Table S4](#). For vetting the specificity of these antibodies against their respective histone

modifications, we identified regions enriched in each histone mark using our ChIP-seq datasets and confirmed that each antibody did not cross-react with any other.

ChIP-seq and data analysis

Deep sequencing of immunoprecipitated chromatin was performed using the Illumina HiSeq 2500 system. Sequencing libraries were made using the NEBNext ChIP-Seq Library Prep Master Mix Set for Illumina (New England Biolabs). Single-end, 100-bp sequence reads were trimmed based on read length and read quality using the FASTX tool kit and aligned to the mouse genome (UCSC mm10) using Bowtie v2.2.4 ([Langmead and Salzberg, 2012](#)). All redundant reads were removed from further analysis. SAM files were converted to the BAM format using SAMtools (v0.1.19) ([Li et al., 2009](#)). Peak calling for ND1 was performed using MACS version 1.4.1 with default parameters and the input library as control ([Zhang et al., 2008](#)). Genomic annotation of the peaks identified from the ChIP-seq data was performed using GREAT ([McLean et al., 2010](#)). Density profiles of chromatin marks around ND1-bound sites were computed with Ngsplot using max option ([Shen et al., 2014](#)). For boxplot analysis, the mouse genome was partitioned into 500-bp bins, and signal enrichment was calculated as reads per kilobase per million mapped reads. The consensus sequence was identified by importing a 200-bp sequence surrounding the summit of the peak of ND1 into the MEME program ([Bailey et al., 2009](#)). Microglial enhancer regions were defined by co-occupancy of the histone marks H3K4me1 and H3K27ac.

WGBS and data analysis

Genomic DNA was subjected to bisulfite treatment with the EZ DNA Methylation-Gold Kit (ZYMO Research) according to the manufacturer's instructions. In this study, we adopted a strategy termed post-bisulfite adaptor tagging (PBAT), which provides an unbiased methylome analysis ([Miura et al., 2012](#)). The multiplex PBAT method is described in detail on the CREST/IHEC Japan webpage (<http://crest-ihec.jp/english/epigenome/index.html>) ([Miura et al., 2012](#)). Libraries were synthesized according to this protocol. Briefly, bisulfite-treated DNA was annealed to double-stranded DNA using Klenow fragment (New England Biolabs) with random primers containing 5' biotin tags and an Illumina adaptor (BioPEAN4: 5'-ACACTTTCCCTACACGACGCTTCCGATCTNNNN-3'). The biotinylated molecules (first strand) were captured using Dynabeads M280 Streptavidin (Invitrogen) and reannealed to double-stranded DNA again using Klenow fragment with random primers containing an Illumina adaptor (PE reverse-N4: 5'-CAAGCAGAA GACGGCATACGAGATNNNN-3'). Finally, template DNA was synthesized as cDNA with a second strand with Illumina primer 3 (5'-AATGATACGGCGACCACCGAGATCTACACTCTTCCCTACACGACGCTTCCGATCT-3'). The PBAT library was quantified using the KAPA library quantification kit (KAPA Biosystems) and sequenced on a Hiseq 2500 (Illumina) as described ([Miura et al., 2012](#)). PBAT single-end reads were mapped to the mouse mm10 reference genome using BMap software (<http://itolab.med.kyushu-u.ac.jp/BMap/index.html>) ([Miura et al., 2012](#)) with default parameter settings. We utilized WGBS data composed of more than 0.98 billion reads, with 72% of CpG sites in the mouse genome covered by at least five reads. The consensus sequence was identified by importing a 200-bp sequence surrounding the CpG sites into the MEME program. Microglia-specific hypomethylated sites were defined as sites that were weakly methylated in microglia (methylation level < 0.2) and highly methylated in other CNS cells (neurons, astrocytes, oligodendrocytes; methylation level > 0.8). WGBS data from neurons, astrocytes and oligodendrocytes were obtained from our previous study ([Sanosaka et al., 2017](#)). To reveal the enrichment of immune-related factors in hypermethylated CpG sites in iN cells, we used ChIP-Atlas ([Oki et al., 2018](#)) and public ChIP-seq data obtained from macrophages ([Kaikkonen et al., 2013; Langlais et al., 2016; Mancino et al., 2015; Menéndez-Gutiérrez et al., 2015; Ng et al., 2011; Ostuni et al., 2013; Soucie et al., 2016](#)).

Microglial ablation

To pharmacologically ablate brain microglia, mice were fed PLX5622-formulated D12450J diet (1.2 mg PLX5622 per kg of diet, Research Diets) *ad libitum* during 4 weeks.

Stereotactic brain injections

The human CD68 promoter ([Iqbal et al., 2014](#)) was cloned into the lentiviral vector FG12 (Addgene) using XbaI and Xhol sites. ND1-P2A was then cloned and replaced with the UbiC promoter using Xhol and AgeI sites. Lentivirus was concentrated by Lenti-X (Clontech). Striata of adult mice were stereotactically injected with 1.5 μL virus with a titer of $0.5\text{--}2 \times 10^9$ particles per milliliter. Injection coordinates were as follows: anterior/posterior, +1.0 mm; medial/lateral, ± 2 mm; and dorsal/ventral from skull, −3.0 mm.

Immunohistochemistry

Adult mouse brains were fixed in 4% paraformaldehyde and 40-μm sections were cut with a cryostat (Leica). Cryosections were washed with PBS and blocked for 1 h at RT with blocking solution (5% FBS, 0.3% Triton X-100), and incubated overnight at 4°C with primary antibodies diluted in blocking solution. The following primary antibodies were used in this study: anti-NeuN (1:500), anti-Iba1 (1:500), anti-βIII-tubulin (1:500), anti-Map2ab (1:500), anti-Tmem119 (1:500), anti-DARPP32 (1:500), anti-PSD95 (1:500), anti-VGLUT1 (1:500) and anti-GFP (1:500). Stained sections were visualized with a confocal microscope (LSM800, Zeiss).

Electrophysiology

Electrophysiological experiments were performed as previously described (Kawano et al., 2017). Briefly, spontaneous and evoked action potentials were recorded using a patch clamp amplifier (MultiClamp 700B; Molecular Devices) in the whole-cell configuration under the current-clamp condition at RT. The evoked action potentials were elicited in response to a somatic depolarization step pulse (100 ms) from the patch pipette (0 pA to 570 pA, Δ30 pA). On the other hand, spontaneous miniature postsynaptic currents (mPSC) were recorded in the whole-cell configuration under the voltage-clamp condition at a holding potential (V_h) of -70 mV at RT. Patch pipette resistance was 4–5 MΩ. Access resistance was not compensated for when recording mPSCs. Data were recorded at a sampling rate of 10 kHz, and filtered at 10 kHz. Data were analyzed offline using Axograph X 1.5.4 software (Axograph Scientific). The mPSCs were detected with an amplitude threshold of 5 pA. For mPSC analysis, events were detected automatically, and then manually inspected to exclude false-positive events. All traces were visually examined to protect against software errors. The standard extracellular solution for patch-clamp experiments was (in mM): NaCl 140, KCl 2.4, HEPES 10, glucose 10, CaCl₂ 2, MgCl₂ 1, pH 7.4, with an adjusted osmotic pressure of 315–320 mOsm. Patch pipettes were filled with an intracellular solution composed of (in mM): KCl 146.3, MgCl₂ 0.6, ATP-Na₂ 4, GTP-Na₂ 0.3, creatine phosphokinase 50 U/ml, phosphocreatine 12, EGTA 1, HEPES 17.8, pH 7.4. When recording mPSCs, TTX (Wako) was added to the standard extracellular solution. All chemicals were purchased from Sigma, except where otherwise specified.

For ex vivo electrophysiology, striatum slices were cut into 200 μm-thick sections with a VT1000 vibratome (Leica) using ice-cold cutting solution consisting of (in mM) 234 sucrose, 2.5 KCl, 1.25 NaH₂PO₄, 10 MgCl₂, 0.5, CaCl₂, 25 NaHCO₃, 11 glucose and myo-inositol. A whole-cell patch-clamp recording was performed in voltage-clamp mode on EGFP-positive cells according to a similar method described previously (Hayashi et al., 2016). Signals were recorded using a patch-clamp amplifier (Axopatch200B; Molecular Devices). The external solution consisted of (in mM) 125 NaCl, 2.5 KCl, 1.25 NaH₂PO₄, 2 MgCl₂, 1.6 CaCl₂, 10 glucose and 25 NaHCO₃ saturated with 95% O₂ and 5% CO₂. Patch pipettes (8–10 MΩ) were filled with an internal solution of (in mM) 120 K-gluconate, 10 HEPES, 0.2 EGTA, 20 KCl, 2 MgCl₂, 7 Na₂-phosphocreatine, 4 Mg-ATP and 0.3 Na₂-GTP, pH adjusted to 7.3 with KOH. Spontaneous excitatory postsynaptic currents (EPSCs) and inhibitory postsynaptic currents (IPSCs) were recorded at a holding potential of -70 mV and 0 mV, respectively, in the presence 10 μM bicuculline methiodide (a GABA_A receptor antagonist). The evoked action potentials were recorded in current-clamp mode. Current steps (0–120 pA, increasing in increments of 10 pA) were applied for 500 ms. The spontaneous EPSCs, IPSCs and evoked action potentials were analyzed by Mini Analysis Program (Synaptosoft) and Clampfit (Molecular Devices). For biocytin labeling, intracellular solution was supplemented with 0.3% biocytin (Vector Laboratories, SP-1120).

QUANTIFICATION AND STATISTICAL ANALYSIS

No statistical methods were used to pre-determine sample sizes. The statistical analyses were done afterward without interim data analysis. No data points were excluded. We do not use any methods to determine whether the data met assumptions of the statistical approach. All data were collected and processed randomly. Unpaired Student's t tests and the Wilcoxon rank sum test were used to calculate the p value for pairwise comparisons. For multiple comparisons, p values were calculated using one-way ANOVA with the Tukey post hoc test and Wilcoxon rank sum test. The significance of the enrichment of transcription factors in indicated regions or sites was determined using the hypergeometric distribution. The exact values of n (sample size) are provided in the figures and figure legends. We considered a p value less than 0.05 to be statistically significant. Data represent mean + SEM.

DATA AND SOFTWARE AVAILABILITY

The RNA-Seq, WGBS and ChIP-seq data obtained in this study have been uploaded to NCBI GEO datasets, under accession number GSE104435.